AD-A189 870 THE AGE HARDENING RESPONSE OF THERMOMECHANICALLY PROCESSED AL-MG-LI ALLOYS(U) NAVAL POSTGRADUATE SCHOOL MONTEREY CA W F FERRIS DEC 87 1/1

UNCLASSIFIED F/G 11/6 1 NL

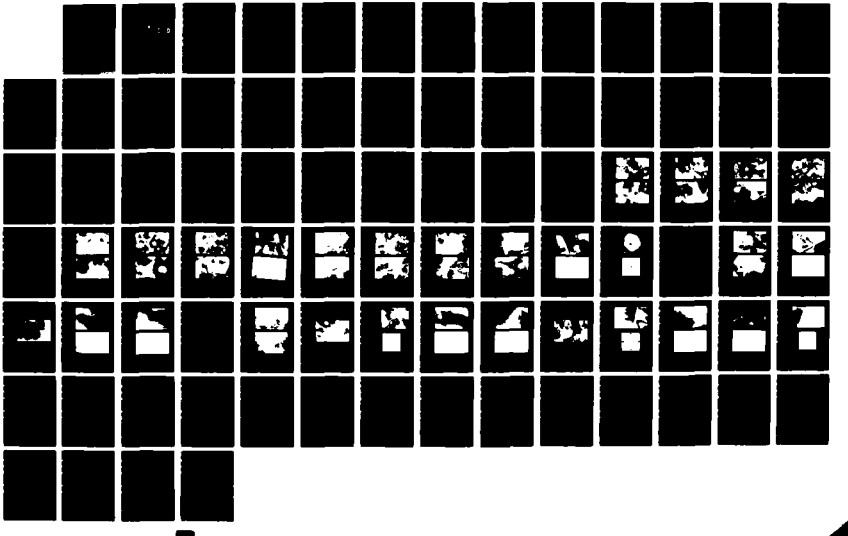

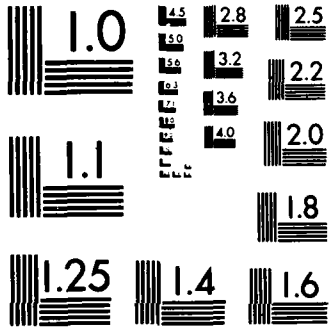

MICROCOPY RESOLUTION TEST CHART
NATIONAL BUREAU OF STANDARDS-1963-A

NAVAL POSTGRADUATE SCHOOL

Monterey, California

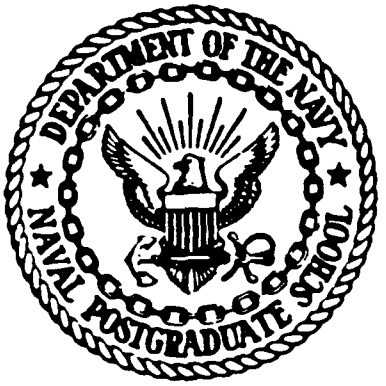

THESIS

THE AGE HARDENING RESPONSE OF
THERMOMECHANICALLY
PROCESSED AL-MG-LI ALLOYS

by

William F. Ferris

December 1987

Thesis Advisor T.R. McNelley
Co-Advisor S.J. Hales

SECURITY CLASSIFICATION OF THIS PAGE

REPORT DOCUMENTATION PAGE

1a REPORT SECURITY CLASSIFICATION: UNCLASSIFIED	1b RESTRICTIVE MARKINGS
2a SECURITY CLASSIFICATION AUTHORITY	3 DISTRIBUTION/AVAILABILITY OF REPORT: Approved for public release, distribution is unlimited.
2b DECLASSIFICATION/DOWNGRADING SCHEDULE	
4 PERFORMING ORGANIZATION REPORT NUMBER(S)	5 MONITORING ORGANIZATION REPORT NUMBER(S)
6a NAME OF PERFORMING ORGANIZATION: Naval Postgraduate School; 6b OFFICE SYMBOL (If applicable): 67	7a NAME OF MONITORING ORGANIZATION: Naval Postgraduate School
6c ADDRESS (City, State, and ZIP Code): Monterey, CA 93943-5000	7b ADDRESS (City, State, and ZIP Code): Monterey, CA 93943-5000
8a NAME OF FUNDING/SPONSORING ORGANIZATION; 8b OFFICE SYMBOL (If applicable)	9 PROCUREMENT INSTRUMENT IDENTIFICATION NUMBER
8c ADDRESS (City, State, and ZIP Code)	10 SOURCE OF FUNDING NUMBERS: PROGRAM ELEMENT NO; PROJECT NO; TASK NO; WORK UNIT ACCESSION NO

11 TITLE (Include Security Classification)

THE AGE HARDENING RESPONSE OF THERMOMECHANICALLY PROCESSED AL-MG-LI ALLOYS

12 PERSONAL AUTHOR(S)

William E. Ferris

13a TYPE OF REPORT	13b TIME COVERED	14 DATE OF REPORT (Year, Month, Day)	15 PAGE COUNT
Master's Thesis	FROM _____ TO _____	1987 December	85

16 SUPPLEMENTARY NOTATION

17 COSATI CODES			18 SUBJECT TERMS (Continue on reverse if necessary and identify by block number)
FIELD	GROUP	SUB-GROUP	Aluminum-magnesium-lithium Alloys, Thermomechanically Processed, Superplasticity, Age Hardening Studies, Aluminum alloys, Magnesium alloys, Lithium alloys

19 ABSTRACT (Continue on reverse if necessary and identify by block number)

Four Al-Mg-Li alloys of compositions (weight percent) in the ranges 6-8% Mg, 0.5-2% Li, and 0.15-0.25% Zr were hot forged and warm rolled (thermo-mechanically processed) to achieve a microstructure suitable for superplasticity. They were then subjected to age-hardening studies at temperatures indicated by concurrent differential scanning calorimetry research. Optical and transmission electron microscopy techniques were used to relate microstructure to mechanical properties. Only the 6%Mg-2%Li alloy showed significant age hardening response, however, concurrent research demonstrated excellent superplastic response in the 6%Mg-1%Li and 8%Mg-1%Li alloys.

Keywords:

20 DISTRIBUTION/AVAILABILITY OF ABSTRACT	21 ABSTRACT SECURITY CLASSIFICATION
☑ UNCLASSIFIED/UNLIMITED ☐ SAME AS RPT ☐ DTIC USERS	unclassified

22a NAME OF RESPONSIBLE INDIVIDUAL	22b TELEPHONE (Include Area Code)	22c OFFICE SYMBOL
T.R. McNelley	(408) 646-2589	69Mc

DD FORM 1473, 84 MAR — 83 APR edition may be used until exhausted. All other editions are obsolete.

SECURITY CLASSIFICATION OF THIS PAGE

U.S. Government Printing Office 1986—606-24.

Approved for public release; distribution is unlimited.

The Age Hardening Response of Thermomechanically Processed Al-Mg-Li Alloys

by

William F. Ferris
Lieutenant Commander, United States Navy
B.S., U. S. Naval Academy, 1975

Submitted in partial fulfillment of the requirements for the degree of

MASTER OF SCIENCE IN AERONAUTICAL ENGINEERING

from the

NAVAL POSTGRADUATE SCHOOL
December 1987

Author: William F. Ferris
William F. Ferris

Approved by: T.R. McNelley
T.R. McNelley, Thesis Advisor

Stephen J. Hales
S.J. Hales, Co-Advisor

M. F. Platzer
M. F. Platzer, Chairman,
Department of Aeronautics

G. E. Schacher
Gordon E. Schacher,
Dean of Science and Engineering

ABSTRACT

Four Al-Mg-Li alloys of compositions (weight percent) in the ranges 6-8% Mg, 0.5-2% Li, and 0.15-0.25% Zr were hot forged and warm rolled (thermo-mechanically processed) to achieve a microstructure suitable for superplasticity. They were then subjected to age-hardening studies at temperatures indicated by concurrent differential scanning calorimetry research. Optical and transmission electron microscopy techniques were used to relate microstructure to mechanical properties. Only the 6%Mg-2%Li alloy showed significant age hardening response, however, concurrent research demonstrated excellent superplastic response in the 6%Mg-1%Li and 8%Mg-1%Li alloys.

TABLE OF CONTENTS

LIST OF TABLES

LIST OF FIGURES

ACKNOWLEDGEMENTS

I would like to express my sincere appreciation for the efforts of Professors Terry McNelley and Stephen Hales. Their guidance and instruction were invaluable. Additional gratitude is expressed for the services and assistance provided by the Materials Science technical staff, led by Mr. Tom Kellogg, and to fellow students, General Ahmed Salama (EAF) and Captains Ian Munro (CAF) and Procopios Spiropoulos (HAF) for their help. Finally, special thanks to my loving wife, Patti Jo, for her patience, understanding and sacrifice throughout my studies at the Naval Postgraduate School, and to my daughters, Jennifer and Kathleen, for being themselves.

I. INTRODUCTION

Aluminum alloys are widely used because of their combination of good ductility, moderate to high strength, excellent corrosion resistance in most environments, and low density. According to an American Society for Testing and Materials (ASTM) study cited by Quist, *et al.*, density was far and away the single most important material property in determining the Navy Lockheed S-3's structural weight, more important than strength, stiffness, or durability [Ref. 1].

Lithium is an extremely attractive alloying addition to aluminum. At low concentrations, each weight percent added increases the elastic modulus by about 6% while reducing density by 3% [Ref. 2]. One of the first examples of lithium additions to aluminum alloys was in 1924, when it was used in the German alloy 'Scleron' most probably for alloy patentability, rather than for metallurgical considerations. Aluminum-lithium (Al-Li) alloys were not commercially competitive until 1958, when North American Aviation selected Alcoa's alloy 2020 for the wing skin panels of its new supersonic Navy A-5 heavy attack bomber. Alloy 2020 was lighter (it saved 160 pounds) and stiffer than the 2024 it replaced, but required careful engineering to deal with its fatigue resistance shortcomings [Ref. 3]. More recently, Al-Li alloys have been selected by McDonnell Douglas for use in MD-11 floor beams and in the wing skin panels of a research F-15 [Ref. 4]. The alloy used in the F-15, Alcan's Lital, is 9% lighter and 5% stronger than the alloy it replaced.

It is anticipated that lithium containing aluminum alloys will be extensively used as structural components in the aircraft of the 1990's. Compared to current commercial alloys, Al-Li alloys can be expected to have 5-10% reduced density, 15-20% increased elastic modulus, and 10-15% increased ultimate tensile strength [Ref. 5]. However, because Al-Li alloys are about three times more expensive to fabricate than current alloys, they cannot simply be substituted into aircraft without redesigning components to take advantage of the improved properties. It has been estimated that a Boeing 747-200 transport designed to utilize Al-Li alloys could be 11,500 pounds (about 3%) lighter than the current aircraft [Ref. 6]. Quist, *et al.*, estimated that a large transport will save 15 to 20 gallons of fuel per year per pound of weight eliminated [Ref. 1: p.315]. This yields a conservative fuel savings estimate of 172,500 dollars per year per aircraft.

Recent industrial applications of superplastic forming (SPF) have led to additional weight savings and reduction in fabrication costs. The one step forming of complicated shapes to close tolerances eliminates fasteners and welds, and improves resistance to corrosion and fatigue. Despite greater material costs, SPF can be the least expensive forming method for parts that will not be mass produced due to less expensive tooling and less machining time. However, superplastically formed parts have not been suitable for primary structure because they have only moderate ambient temperature strengths and ductilities. A high strength alloy with the ability to be superplastically formed would bring about major reductions in cost and weight, and increases in performance, over a broad spectrum of applications.

Most recent industrial uses of SPF have been with aluminum and titanium alloys, which have been successfully fabricated for numerous aeronautical applications, among them the oil cooler inlet (Al) for the Navy Lockheed P-3 patrol plane, and for the auxiliary power unit door (Ti) for the Air Force Rockwell B-1 bomber.

Much research has been done at the Naval Postgraduate School (NPS) on superplasticity in aluminum alloys. This research has centered on the moderate temperature superplastic behavior of high-Mg, Al-Mg alloys which have been thermo-mechanically processed at moderate temperature. Four such alloys, containing Li for modulus improvement and further density reduction, were developed at NPS to investigate superplastic response. Oster and Sanchez investigated 8%Mg-0.5%Li and 8%Mg-1%Li alloys with the goal of understanding microstructural evolution, microstructure's influence on superplastic behavior, and superplastic mechanisms. They found the alloys to be moderately superplastic, but to have suffered a loss in strength compared to the corresponding binary alloy [Refs. 7,8]. In a step toward the development of a superplastic alloy of increased strength, this thesis will investigate the age hardening potential of thermomechanically processed Al-Mg-Li alloys.

II. BACKGROUND

A. WROUGHT ALUMINUM ALLOYS

The wide range and many combinations of desirable properties possible in aluminum alloys have made them the most versatile aerospace materials. Wrought aluminum alloys may be categorized broadly into the following two groups, heat treatable alloys and non-heat treatable alloys.

Heat treatable alloys are used in applications for which a high strength-to-weight ratio is required. These alloys include 2024 and 7475, which are generally formed in the annealed condition, then aged to produce the desired mechanical properties in the finished product.

Non-heat treatable alloys derive strength from the presence of alloying elements in solid solution. These alloys possess excellent workability, and are used in applications requiring moderate to high strength. Dislocation substructure introduced during working provides another important element of strength. These alloys usually receive a partial anneal to restore ductility prior to service, and thus are used in a condition called semi- or partially fabricated. Non-heat treatable alloys, such as the 5xxx series, which contain magnesium as the major alloying addition, exhibit good corrosion resistance and excellent welding characteristics.

In order to discuss the behavior of the alloys used in this research, it is necessary to define the various strengthening mechanisms which contribute to achieving optimum mechanical properties. Metals deform through slip processes involving the motion of dislocations through the crystal lattice. The essential goal of strengthening is to impede the motion of dislocations; various methods for achieving this are discussed below.

1. Strain Hardening

Strain hardening (also called work hardening) depends upon the generation of dislocations by plastic deformation. Hardening occurs because the dislocations interact directly among themselves, or indirectly with the stress fields caused by lattice defects. These interactions cause a reduction in the mobility of dislocations, requiring an increase in the stress needed to move them, in other words strain hardening the material [Ref. 9]. Strain hardening is an important contributor to the strength of cold

worked aluminum products, many of which contain magnesium, such as the previously mentioned 5xxx series.

2. **Solid Solution Strengthening**

Aluminum readily dissolves many elements to form solid solutions. The presence of solute atoms creates strain which inhibits dislocation motion by providing a frictional force. The nature of the solid solution is primarily governed by the relative size difference between solute atoms and the aluminum atoms. Elements such as lithium, magnesium, and zirconium have similar atomic dimensions so that they may substitute directly for aluminum atoms in the lattice. Thus, these elements tend to form substitutional solid solutions. Magnesium, for example, is known to form 'clouds' around dislocations which retard mobility and lead to deformation by a solute-drag mechanism. Solid solution strengthening is an element of strengthening for almost all aluminum alloys, and is particularly important in the Al-Mg system.

3. **Grain Size Strengthening**

The yield strength of most crystalline solids increases with decreasing grain size at ambient temperatures. The basic idea behind the separately developed theories of Hall and Petch is that a dislocation pile-up can break through a grain boundary due to stress concentration at the head of the pile-up [Ref. 9: p. 497]. Because a slip plane in a large grain can accommodate more dislocations, generating more stress at the grain boundary, it is more likely to sustain a break-through than is a plane in a smaller grain. The situation changes at elevated temperatures where diffusion becomes a factor. A fine grain size tends to enhance deformation processes such as the grain boundary sliding at work in superplastic deformation (SPD). Where creep resistance is important, a coarser grain structure is desirable, explaining the use of single crystals in such applications as gas turbine blades.

4. **Dispersion Strengthening**

Dispersion strengthening is strengthening that arises from an insoluble second phase that is not formed by precipitation from the solid state. The second phase may be mechanically introduced, or may be an intermetallic compound formed while the alloy is molten. A good example of the latter is the primary Al_3Zr which forms via a peritectic reaction during solidification. When a dislocation moving through the matrix material encounters harder dispersoids, it will not generally be able to cut through them. To pass, the dislocation will have to bow between the dispersoids and around them, leaving a dislocation loop around the particles. The stress required is inversely

related to the distance between particles, thus, for a given volume fraction of dispersoids, a uniform distribution of fine, closely spaced particles will be a more effective strengthener than coarser particles, farther apart.

Another contribution to dispersion strengthening is less easily quantifiable. Usually, the second phase particles act as prolific dislocation sources under stress, and cause the crystalline matrix to become strain hardened. Furthermore, the dispersoids inhibit softening processes such as recovery and recrystallization, allowing property retention at elevated temperature through microstructural stability. [Ref. 10: p.265]

5. **Precipitation Hardening (Age Hardening)**

Precipitation hardening can occur when an alloy contains alloying elements that are more soluble at elevated temperatures than at room temperature. When these alloys are solution heat treated to drive these elements back into solid solution and then rapidly quenched, a supersaturated solid solution is produced. The strength of the alloy is developed as the alloying elements precipitate out of the solution. Coherent precipitates (those that share the same crystal structure and occupy the same lattice as the matrix), such as the δ' (Al_3Li) and secondary Al_3Zr important to this research, are much more effective strengtheners than incoherent precipitates such as β (Al_8Mg_5), δ (AlLi), and primary Al_3Zr. Alloying heat treatments at intermediate temperatures are usually employed to develop peak strength as quickly as possible. Often a working step is included between the solution treatment and aging to introduce dislocations to serve as nucleation sites for a more uniform precipitate distribution. In this work, dislocations are introduced during TMP. Over-aging the material results in a loss of strength as the precipitates grow larger and farther apart, often with concomitant formation of precipitate free zones (PFZ's) on the grain boundaries.

B. GRAIN REFINEMENT FOR SUPERPLASTICITY

1. Grain Refinement

Conventional processing of wrought aluminum alloys is aimed at avoiding the formation of isolated large grains, rather than grain refinement *per se*. This is because it is very difficult to process aluminum alloys to produce a fine grain size in the absence of a very large volume fraction of second phase. For this reason , historically, fine grain sizes have only been achieved in alloys at or near the eutectic or eutectoid composition. Wrought alloys in final product form tend to be in a semi-fabricated condition. Recovery and recrystallization processes lead to a softening of the material, and often to a reduction in the desired mechanical properties.

2. Recovery and Recrystallization

a. Recovery

Recovery is the process in which dislocation networks are rearranged into lower energy configurations without a change in crystal lattice orientation. The stored energy of deformation provides the driving force for recovery, which results in a lower dislocation density. Polygonization is the recovery process in which strain energy is reduced by the formation of a cellular structure with the dislocations confined to regular arrays in the cell walls.

Aluminum is a high stacking fault energy (SFE) material, which allows dislocations to migrate readily on all the active slip planes. The addition of 1% magnesium to aluminum lowers the SFE somewhat, with little further effect for greater additions. Despite the slightly more difficult recovery this brings about, with large amounts of magnesium in solution, recovery processes still dominate, with concurrent inhibition of recrystallization.

b. Discontinuous Recrystallization

Discontinuous recrystallization (DRX) is the process by which new, strain free grains nucleate and grow. Nucleation often occurs at deformation zones adjacent to undeformable particles greater than a critical size, which varies inversely with strain [Ref. 11]. The matrix in these deformation zones is highly distorted, which causes high-angle boundaries to form locally. The high-angle boundary then migrates outward into the deformed lattice along a well defined front, leaving a strain free grain in its wake. The migration driving force, like that of recovery, is the reduction of the stored energy of deformation [Ref. 12].

The grain size resulting from discontinuous recrystallization is controlled by precipitate size and spacing, with a bimodal size distribution of second phase being most desirable for grain refinement. Larger particles provide numerous nucleation sites for new grains, while homogeneous, closely spaced, small particles tend to retard boundary migration. The resultant grain size is directly related to particle spacing [Ref. 13].

c. Continuous Recrystallization

Continuous recrystallization (CRX) is a gradual process for which no entirely satisfactory model exists. It is a mechanism which could be considered to be advanced recovery. There is no recrystallization front, no nucleation and growth of new, strain free grains, and no high-angle grain boundary migration. A mechanism of

low-angle subgrain boundary migration and coalescence into high-angle boundaries has been proposed, but not proven.

Two types of continuous recrystallization have been observed. The first, static continuous recrystallization, requires long annealing times for thermal activation to assist in the reduction of stored energy of deformation. The second type, dynamic continuous recrystallization, relies upon the continued deformation of the material to provide the driving force. Continuous recrystallization permits the development of a more highly refined microstructure than does discontinuous recrystallization.

3. **Processing for Superplasticity**

In order for a material to sustain SPD, it must either possess a uniform, fine, stable, and equiaxed grain structure, or develop such a microstructure during deformation. In order to meet this requirement, grain refinement by careful control of microstructural evolution during TMP is required.

Methods developed by Rockwell for achieving fine-grain superplasticity in Al-Zn-Mg-Cu (7xxx) alloys have centered around heat treatments subsequent to controlled TMP to transform a heavily deformed microstructure into a fine-grained structure via discontinuous recrystallization. An alternative approach has been developed by Superform for producing fine grained Al-Cu-Zr (Supral) alloys capable of sustaining SPD in the absence of prior recrystallization heat treatments. NPS research on the TMP of Al-Mg-Zr alloys has revealed that these materials also behave in a superplastic manner while in a deformed, essentially unrecrystallized condition. The highlights of the various processes are summarized in Table 1 . Due to the proprietary nature of the Superform process details, some values are estimates [Ref. 14].

4. **NPS Alloys**

An alloying element introduced into pure aluminum at a concentration less than the solid solubility limit will result in a single-phase microstructure. Alloying element concentration in excess of the solid solubility limit produces a second phase microconstituent that may consist of an intermetallic compound, or, in certain conditions, consist of the pure alloying element. Additional solutes introduced to form ternary, or higher order alloys, generally cause a reduction in the solid solubility of the the solute atoms below that of the corresponding binary alloy. Excess solute atoms may produce multi-constituent intermetallic compounds. Metastable phases may be present under non-equilibrium conditions. [Ref. 15: p. 6-7]

TABLE 1

PROCESSES FOR SUPERPLASTICITY

Process	Rockwell	Superform	NPS
Alloy composition (Aluminum + ...)	5.5%Zn-2%Mg-1.5%Cu (7475)	6%Cu-0.4%Zr (Supral)	10%Mg-0.1%Zr
Alloy T_m (C)	550	590	520
Homogenization Temperature (C)	482	450	440 + 480
Overaging Temperature (C)	8 hrs. @ 400	--	--
Rolling Temperature (C)	200	450 + 25	300
Recrystallization Temperature (C)	0.25 hrs. @ 482	--	--
SPD Temperature (C homologous)	516, 0.95T_m	460, 0.85T_m	300, 0.7T_m

a. Al-Mg-Zr

Magnesium, as an alloying addition to aluminum, reduces density, ductility, and elastic modulus, but increases hardness, strength, and fatigue resistance. The solid solubility of magnesium in aluminum ranges from 17.4% (all alloying percent values used in this thesis are weight percent unless specified otherwise) at the eutectic temperature of 500°C, to 6.7% at the TMP temperature of 300°C, to 1.9% at room temperature [Ref. 16] (see the Al-Mg phase diagram, Figure 2.1 [Ref. 17]). In addition to the property improvements imparted by solid solution strengthening, Al-Mg alloys can be made to precipitate β. β has a complex cubic structure, with a unit cell comprising about 1,168 atoms which reside at 23 crystallographically different positions [Ref. 18]. The extremely large lattice parameter (2.82 nm) of β makes its diffraction pattern unmistakable. In the study of a 10%Mg-0.1%Zr alloy, Lee, *et al.*, found that β precipitated during the warm rolling phase of TMP, tending to form at grain triple points [Ref. 19]. Hales, *et al.*, found β to exert a stabilizing influence on microstructure by retarding dislocation and grain sub-grain boundary motion, and to deter grain coarsening at elevated temperature by pinning grain boundaries [Ref. 20]. The concentration of magnesium in the alloys studied is higher than that normally found in commercial wrought alloys, with the intent of increasing the volume fraction of β.

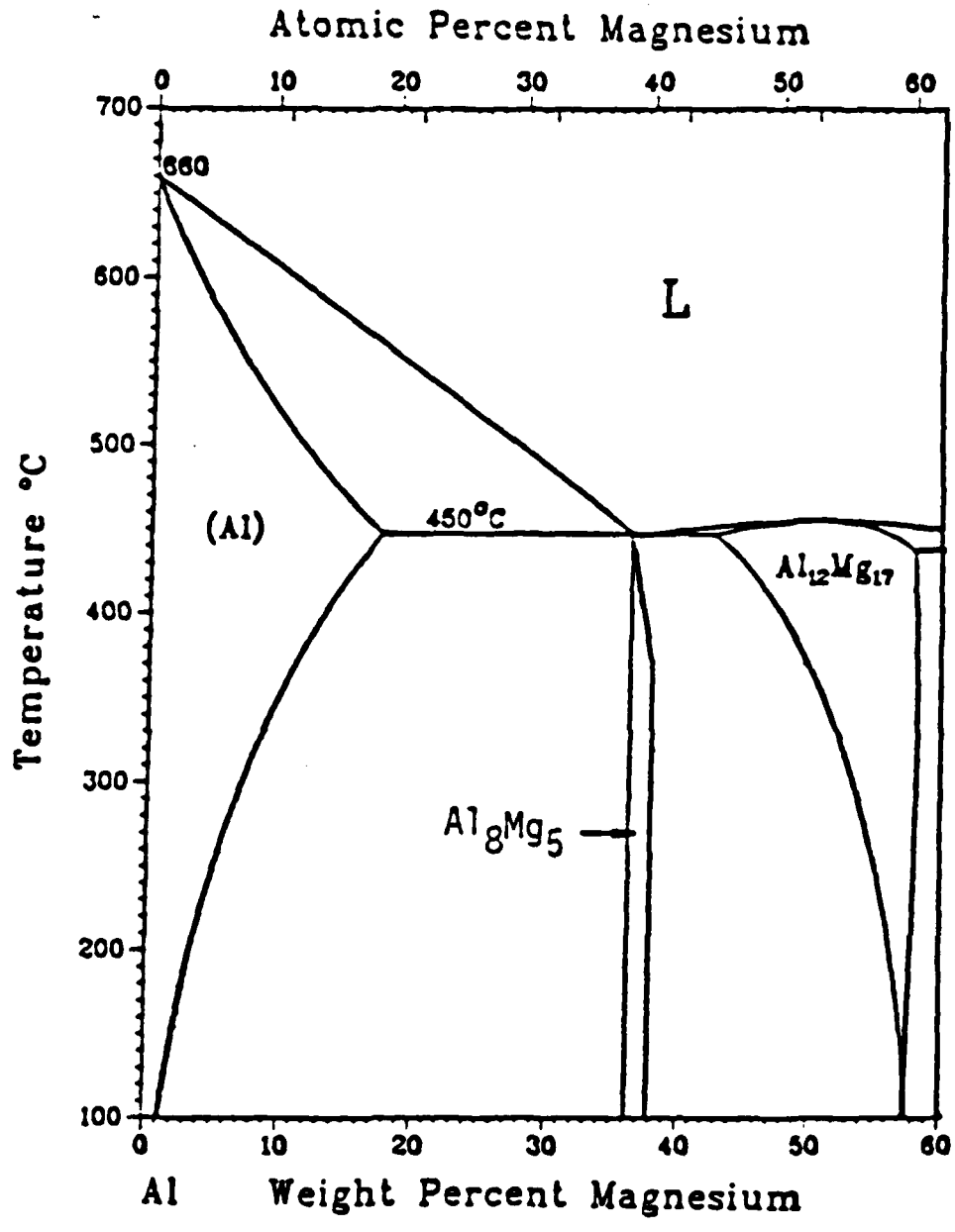

Figure 2.1 Al-Mg Phase Diagram

Zirconium is one of the many ancillary solute additions to aluminum alloys which control grain size and the degree of recrystallization. The solid solubility of zirconium in aluminum ranges from 0.11% at the peritectic temperature of 661°C to about 0.05% at 400°C. The primary (1°) and secondary (2°) forms of Al_3Zr have differing structures, lattice parameters, and morphologies. Primary Al_3Zr has a tetragonal structure, and forms through the peritectic reaction on solidification as relatively large, cuboidal precipitates. Primary Al_3Zr contributes minimal strengthening and ties up zirconium that could better serve in secondary Al_3Zr. Secondary Al_3Zr has a cubic structure and forms as fine, spheroidal, coherent, and oriented precipitates, which are effective at inhibiting recrystallization in regions where they occur. However, due to zirconium's relatively low diffusivity in aluminum, and the peritectic reaction it undergoes on solidification, inhomogeneous distributions of Al_3Zr are common [Ref. 21].

b. Al-Li

Lithium, as an alloying addition to aluminum, increases elastic modulus while decreasing density. The solid solubility of lithium in aluminum (see the Al-Li phase diagram, Figure 2.2 [Refs. 22,23: pp. 1027, 128]) ranges from 4.2% at the eutectic temperature of 602°C, to 1.5% at the rolling temperature of 300°C, to about 0.8% at the lower aging temperature of 120°C [Ref. 16: p.308]. The precipitation reaction,

supersaturated solid solution ----> δ'----> δ

produces the fine, spheroidal δ' that confers age hardening. The δ' is metastable and coherent, with a structure of the $L1_2$ superlattice type. The reaction, when allowed to continue, also produces the equilibrium, incoherent δ which reduces strength on overaging. At lithium concentrations above about 1.7%, δ' formation cannot be suppressed even with a cold water quench [Ref. 24]. Appropriate heat treatments can optimize δ' size, distribution, and volume fraction for maximum precipitation hardening. At Li concentrations below about 1.6 percent, δ' formation has not been found [Ref. 25].

Secondary Al_3Zr in Al-Li alloys is very effective at inhibiting recrystallization, and tends to raise yield strength. Additionally, Al-Li-Zr alloys age more rapidly and achieve higher peak strengths than corresponding Al-Li-Mn alloys.

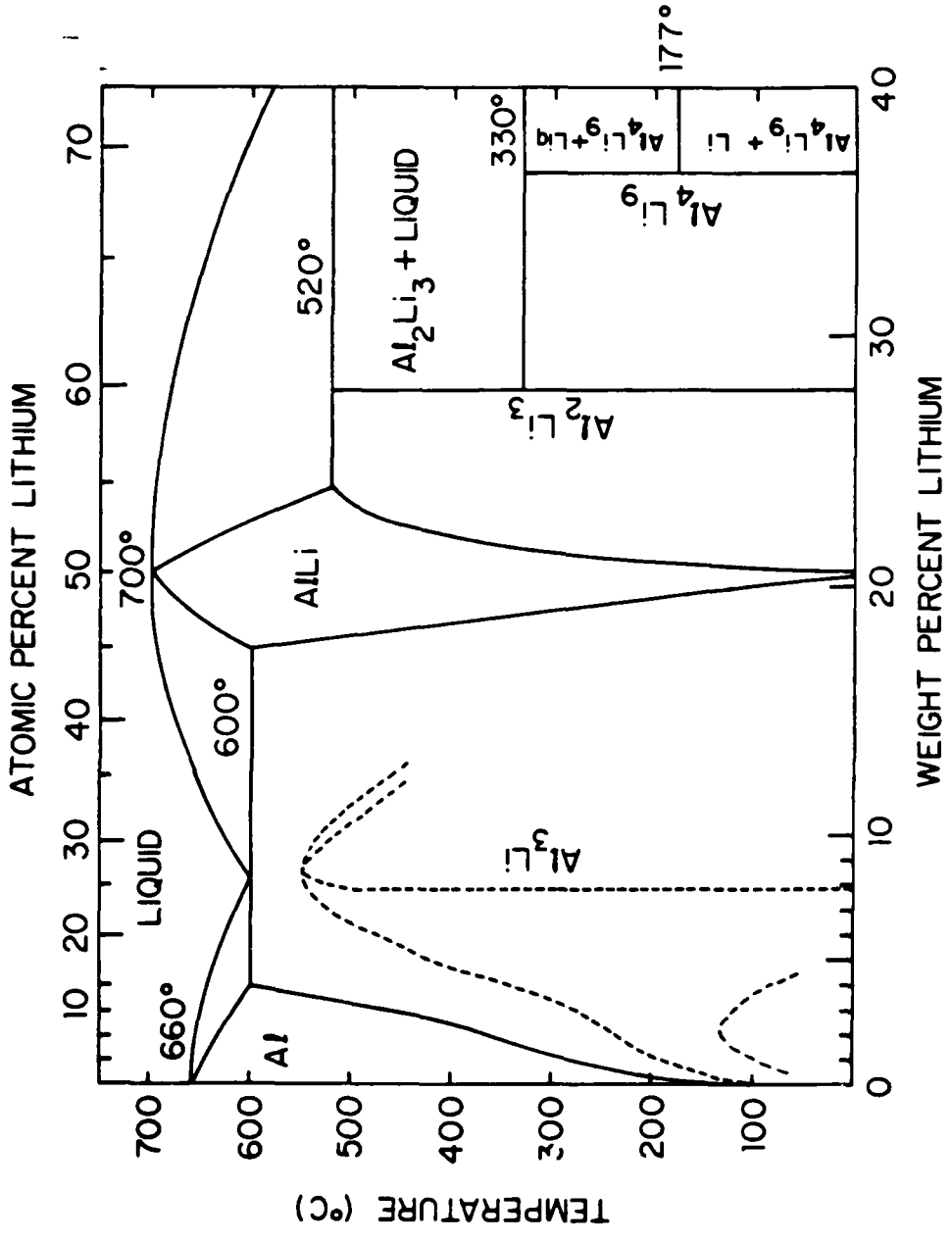

Figure 2.2 Al-Li Phase Diagram

Composite precipitation, in which δ′ nucleates on Al_3Zr particles, in addition to within the matrix, has been observed in Al-Li-Zr systems. [Ref. 26]

Gayle and Vander Sande have proposed that lithium is incorporated into the zirconium sublattice in the Al_3Zr, modifying the atomic scattering factors so that the structure factor is nearly zero. This accounts for the difficulty of obtaining bright dark field TEM images of Al_3Zr [Ref. 27].

c. Al-Mg-Li-Zr

The addition of Li to the Al-Mg-Zr system significantly reduces density, increases elastic modulus, but reduces strength [Ref. 7: p. 68]. Magnesium additions reduce the solubility of lithium, while lithium additions restrict the field of existence of the β phase, and at the same time expand the $Al_{12}Mg_{17}$ phase field at elevated temperature [Ref. 28]. In the alloys studied in this research (see Figure 2.3 and Table 2 for the Al-Mg-Li phase diagram [Ref. 16: p. 555]), multi-constituent phases include $Al_3(Li,Zr)$, Al_2MgLi, and $Al_{12}Mg_{17}$, in which Li may substitute for some of the Mg up to $Al_4Mg_3Li_2$ [Ref. 16: p. 312]. The precipitation sequence,

supersaturated solid solution ----> δ′----> Al_2MgLi

is similar to the binary Al-Li reaction. Thompson and Noble [Ref. 29] found Al_2MgLi to precipitate as long (up to 2 μm), coarsely dispersed rods or laths, which contribute little to strength. Aging at higher temperatures, or overaging, produces Al_2MgLi at the expense of δ′, reducing strength. The relatively high concentration of magnesium in the alloys studied here, in conjunction with the lithium present, is intended not only to increase the volume fraction of β, as in the binary alloy, but also to increase the volume fraction of δ′ by reducing lithium's solid solubility.

d. NPS Research and Goals

(1) *Minor Li Additions (Quasi-Binary Alloys).* A large body of research has been conducted at NPS on superplasticity in high-Mg, Al-Mg-Zr alloys. A TMP that achieves a microstructure capable of sustaining superplastic elongations in excess of 1000% has been developed. In order to increase the density reduction achieved with magnesium additions, and to assess the effect on superplastic response, small amounts of lithium were added. These minor additions have allowed the alloys to behave much like the well-studied Al-Mg-Zr alloys, while reducing density significantly, from 2.57 g cm^3 for the Al-10%Mg alloy, to 2.52 g cm^3 for the 8%Mg-1%Li alloy.

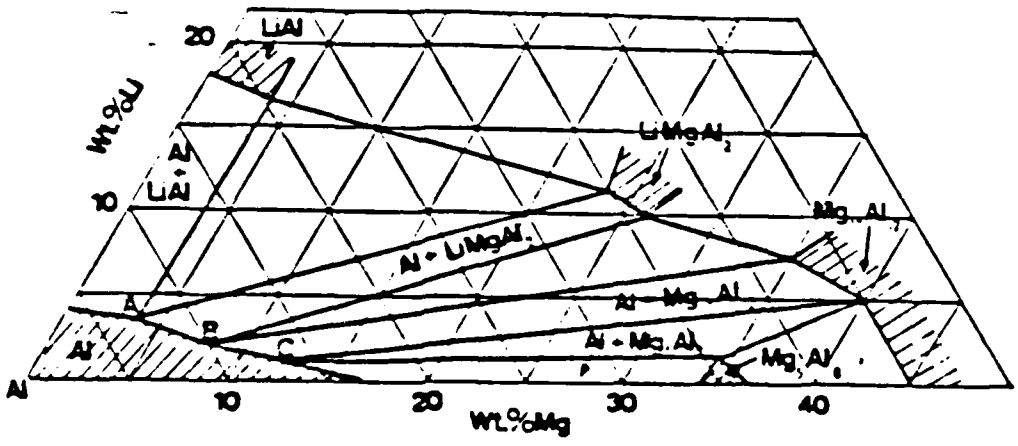

Figure 2.3 Aluminum Corner of the Al-Mg-Li Phase Diagram at 425°C

TABLE 2

APEXES OF AL-MG-LI TERNARY PHASE FIELDS

	425°C		300°C		200°C		150°C	
	%Li*	%Mg	%Li	%Mg	%Li	%Mg	%Li	%Mg
(A)	2.2	3.0	1.5	2.4	1.0	2.0	0.8	1.9
(B)	1.2	7.0	0.7	5.0	0.3	3.4	0.1	3.0
(C)	0.5	12.5	0.3	7.5	0.2	3.6	0.2	1.8

* All percent values are weight percent.

Apex	Phase Field
(A)	$Al + AlLi + Al_2MgLi$
(B)	$Al + Al_2MgLi + Al_{12}Mg_{17}$
(C)	$Al + Al_8Mg_5 + Al_{12}Mg_{17}$

The density of the binary alloy was estimated using the lattice parameter data of Luo, *et al.*, [Ref. 30] the density of the 8%Mg-1%Li alloy was estimated using data from Fridlyander, *et al.*, Thompson and Noble, and Noble, *et al.*, [Refs. 25,29,31]. These additions also provide the potential for age hardening through the precipitation of δ' caused by the high magnesium content forcing lithium out of solution [Ref. 32].

(2) *Larger Li additions (Ternary Alloys).* Larger additions of lithium added to form the 6%Mg-2%Li alloy raise two questions. Does it behave the same as the lower lithium alloys? Will it age harden? The goal of this research is, through alloying additions and TMP, to achieve a grain refined alloy capable of undergoing SPF, and then attaining high strength through heat treatment.

III. EXPERIMENTAL

A. MATERIAL PROCESSING

The Naval Surface Weapons Center, White Oak, Maryland cast ingots as frustums of a cone with a height of 17 cm and a maximum base diameter of 10 cm. Al (99.99% pure) was induction melted in a graphite crucible, with Mg and Li added as pure metal bars. Zr was added using an Al-Zr master alloy. The ingots were cast and solidified under an argon atmosphere due to Li's reactivity. The nominal compositions (in weight percent) of the four alloys studied were Al-6%Mg-1%Li-0.25%Zr, Al-6%Mg-2%Li-0.15%Zr, Al-8%Mg-0.5%Li-0.20%Zr, and Al-8%Mg-1%Li-0.15%Zr. A 0.6 cm disk, for analysis, was cut perpendicular to the long axis near the center of the ingot so that the remaining frustums were of equal volume. Coupons of the Al-8%Mg-0.5%Li-0.2%Zr alloy from five different radial positions of the center disk were analyzed by atomic absorption and x-ray techniques by Anamet Laboratories, Berkeley, California [Ref. 33]. Deviations of the concentrations of Mg, Li, and Zr from the nominal compositions were verified to be within acceptable tolerances. Because the other ingots were prepared similarly by the same facility, their compositions were assumed to be of similar accuracy and homogeneity.

1. Thermomechanical Processing

The 8%Mg billets were solution treated at 440°C for eight hours and at 480°C for sixteen hours to drive all Mg and Li back into solution. The 6%Mg billets were treated likewise, with the exception that 500°C was substituted for 480°C to take advantage of the faster kinetics allowed by the higher liquidus. All billets were hot worked at 480°C to about 3:1 reduction by upset forging to 2.5 cm height on heated platens; the billets were then re-solution treated for one hour at 480°C (8%Mg) or 500°C (6%Mg), and cold water quenched. The 8%Mg, and the 6%Mg-1%Li billets were subsequently isothermally deformed at 300°C by warm rolling to a final true strain greater than 2.5, calculated using Equation 3.1.

$$\varepsilon = \ln (t_i \quad t_f) \qquad \text{(eqn 3.1)}$$

where t_i is the initial thickness, and t_f the final thickness. The billets were reduced 2.5

mm per pass, with thirty minutes of reheating between rolling passes. With the exception of the rolling temperature being 350°C, the 6%Mg-2%Li billets were processed similarly. At the completion of rolling, the strips were cold water quenched. A schematic of the TMP is presented as Figure 3.1.

2. **Coupon Geometry**

In order to provide a minimum of three indenter diameters between hardness test indentations, and between indentations and the edge of the coupon, according to ASTM standard [Ref. 34] using the least amount of material, square coupons of 1.7 cm per side nominal size were cut from each strip. Wafer thicknesses after the sectioning described in Section C. of this chapter were also in accordance with ASTM standard.

B. HEAT TREATMENT

Following TMP and cutting, the coupons were annealed for one hour at the rolling temperature to approximate the time at elevated temperature that might be experienced during superplastic forming, followed by a cold water quench. Two batches of 6%Mg-1%Li coupons received differing treatments in order to ascertain the grain size contribution to strengthening. They were recrystallized at 350°C or 450°C for thirty minutes prior to undergoing aging treatment at 150°C.

The aging temperature for the 6%Mg-2%Li alloy was determined from solvus data calculated by Munro from data gathered in his concurrent Differential Scanning Calorimetry (DSC) research. DSC peaks corresponding to the precipitation of δ' in the three lower lithium alloys were not found, so that the δ' solvus determined by Sigli and Sanchez [Ref. 22: p. 1027] was used to set aging temperatures. Munro's research confirmed that the rolling temperatures were below the β solvi for all the alloys. [Ref. 35]

Cenco 95050 Constant Temperature Apparatus furnaces were used for all heat treatments. A 23 cm x 35 cm x 0.6 cm steel plate at the mid-plane of each furnace was used to support the beakers containing the coupons, to more evenly distribute the heat by conduction, and to provide thermal mass to minimize temperature fluctuations caused by door opening and thermal element cycling. Furnace temperatures were 100°C, 120°C, and 150°C, all plus or minus three degrees. Heat treatment times were 0.3, 3, 10, 24, 72, and 168 hours, roughly evenly spaced on the log scale. The 6%Mg coupons were aged to provide an additional data point at 480 hours.

When furnace temperatures were stable, the 0.3 and 1 hour samples were placed inside separately to maintain a more constant temperature over the short heat

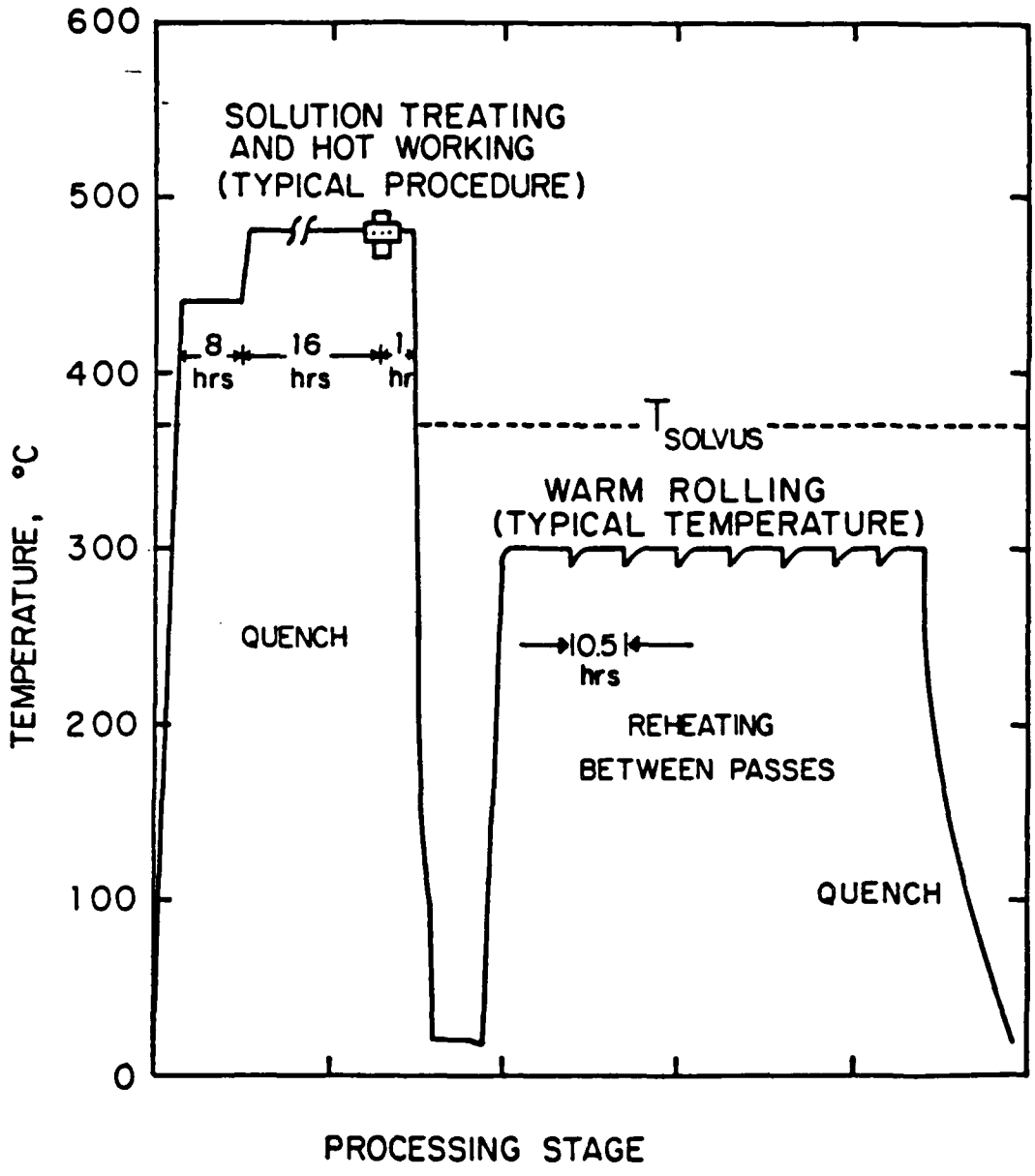

Figure 3.1 TMP Schematic Diagram

treatment period. On completion of the one hour treatment, all remaining coupons were placed in the furnaces simultaneously. All coupons were cold water quenched on completion of their respective heat treatments. Between all stages of processing and throughout the research, all billets, strips, and coupons were stored at -15°C to suppress diffusion.

C. HARDNESS TESTING

All hardness testing was conducted on the Wilson Rockwell Hardness Tester machine. The Rockwell B scale (100 kilogram load, 1/16" indenter, and pedestal anvil) was used. The tester was calibrated using a brass block of known hardness, and found to be reading 1.2 high. A correction of -1.2 was applied to all subsequent hardness readings. Uncertainty in the hardness readings is about 5% [Ref. 16: p.71].

After quenching, the coupons were sectioned parallel to the long transverse plane on a low speed diamond wheel. Both surfaces of one wafer were mechanically ground to 240 grit to remove scale and to provide a planar surface for consistent hardness readings. The other wafer was saved for metallography. Hardness tests (a minimum of five readings, three indenter diameters or more from the edge or another indentation) were done on the former interior plane of the coupon. Readings were averaged to provide one data point.

D. METALLOGRAPHY

1. Optical Microscopy

Specimens were mechanically ground on successively finer grit silicon carbide paper to a planar surface. They were then polished to a scratch-free surface with three-micron diamond paste followed by magnesium oxide using standard metallographic techniques [Ref. 36]. The specimens were then electrolytically polished to provide an undisturbed surface for viewing. The samples were connected as the anode across a constant ten vdc potential in 20% HNO_3 in methanol at 0°C.

Following electro-polishing, the samples were electrolytically etched to provide surface detail. The samples were immersed in Graff-Sargent's reagent at room temperature, connected as anodes across a ten vdc potential, and etched for two to five seconds.

2. Transmission Electron Microscopy

a. Sample Preparation

Blanks were cut from the microscopy wafer and reduced to about 35

micron thickness by mechanical grinding on fine grit silicon carbide paper. Each blank was given a final surface cleaning in 30% HNO_3 in methanol, and rinsed in methanol. Thin foil specimen disks 3mm diameter were prepared with a Struers polisher using 20% HNO_3 in methanol at -20°C, across a potential of 15 vdc. The specimens were examined in the JEOL 120 CX transmission electron microscope operating at 120 kv.

b. Microscopy

The TEM was used in the selected area diffraction (SAD) mode to orient the sample to the desired imaging condition. A two-beam condition was established for conventional bright-field dark-field (BF DF) imaging. In addition, g 3g conditions were established for weak beam DF (WBDF) imaging of structural defects such as dislocations and strain fields around precipitates. [Ref. 37]

The imaging of δ' was conducted using DF centered on a superlattice reflection. The structure and precipitate morphology of δ' are well documented [Refs. 38,39], making the identification of the phase easy. In instances where the identity of the second phase was uncertain, individual precipitates were oriented at major crystallographic poles, such as [100], [110], and [111]. The amount of information available on the precipitation sequences in these types of alloys allowed the identification of the nature of the unknown second phases by obtaining one major zone axis pattern in SAD mode, and subsequently analyzing to determine lattice parameter. The large lattice spacing of the β phase (a = 2.82 nm) allowed for its elimination in determining the nature of other unknown second phases. [Refs. 40,41]

IV. RESULTS

A. HARDNESS DATA

The age hardening response of the 8%Mg-0.5%Li alloy is presented graphically as Figure 4.1, and in tabular form (with all the other alloys' tabular results) in Appendix A. On all curves, the annealed hardness is represented as a straight line for reference. The 8%Mg-0.5%Li alloy displayed no significant response to the heat treatment, neither precipitation hardening, nor softening through recovery, recrystallization, and grain growth.

The 8%Mg-1%Li alloy's hardness curve (Figure 4.2) displays more data scatter than the other curves, but shows no trend after a small initial jump over the annealed hardness.

The 168-hour samples of both 8%Mg alloys had additional uncertainty introduced when the thermostat of the 100°C oven failed between 110 and 120 hours. The temperature rose to 200°C for a period of not more than ten hours. Upon discovery, power was secured, and the door opened to rapidly reduce the temperature to 100°C, whereupon the oven was returned to normal operation. Because the intent was to achieve an overaged condition, and because the data points correlate well with previous points, they have been included.

The 6%Mg-1%Li (see Figure 4.3) alloy displayed a slight hardening response at long aging times. The 150°C curve peaked at 168 hours, and was overaged by 480 hours, when it returned to the annealed hardness. The 120°C curve shows a slower response, but the hardness is still increasing at 480 hours.

Two batches of the 6%Mg-1%Li alloy received recrystallization heat treatments prior to aging to estimate grain size contributions to hardness. The samples recrystallized at 350°C showed a noticeable hardening effect (see Figure 4.4), regaining the hardness of the annealed samples at 168 hours. The 450°C recrystallized samples showed a lesser response. Due to time constraints, the determination of grain size by optical microscopy was not done.

The 6%Mg-2%Li alloy (see Figure 4.5) displayed a significant age hardening response. The 150°C curve peaked at a shorter time and lower hardness than the

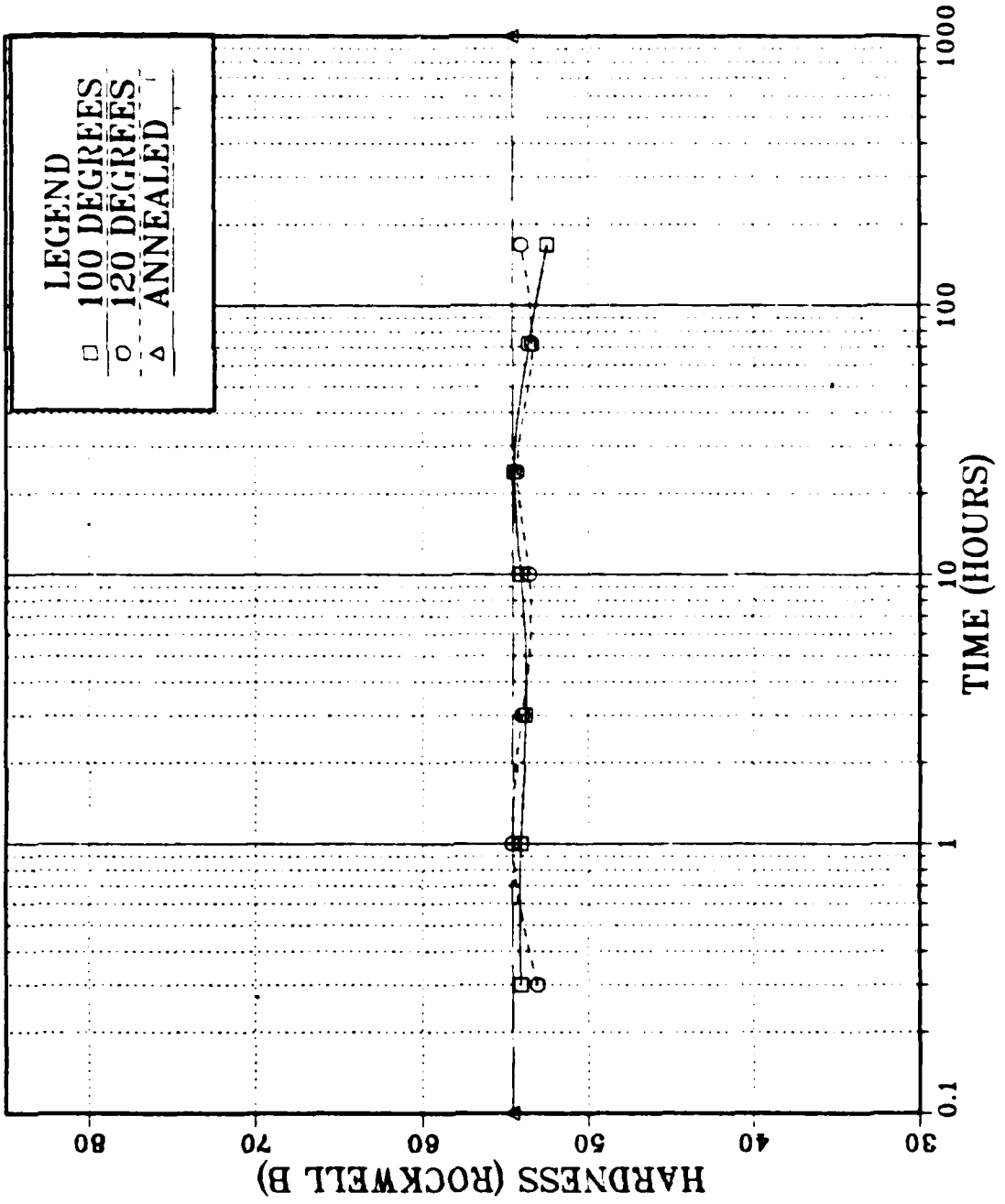

Figure 4.1 Age Hardening Response of the 8%Mg-0.5%Li Alloy

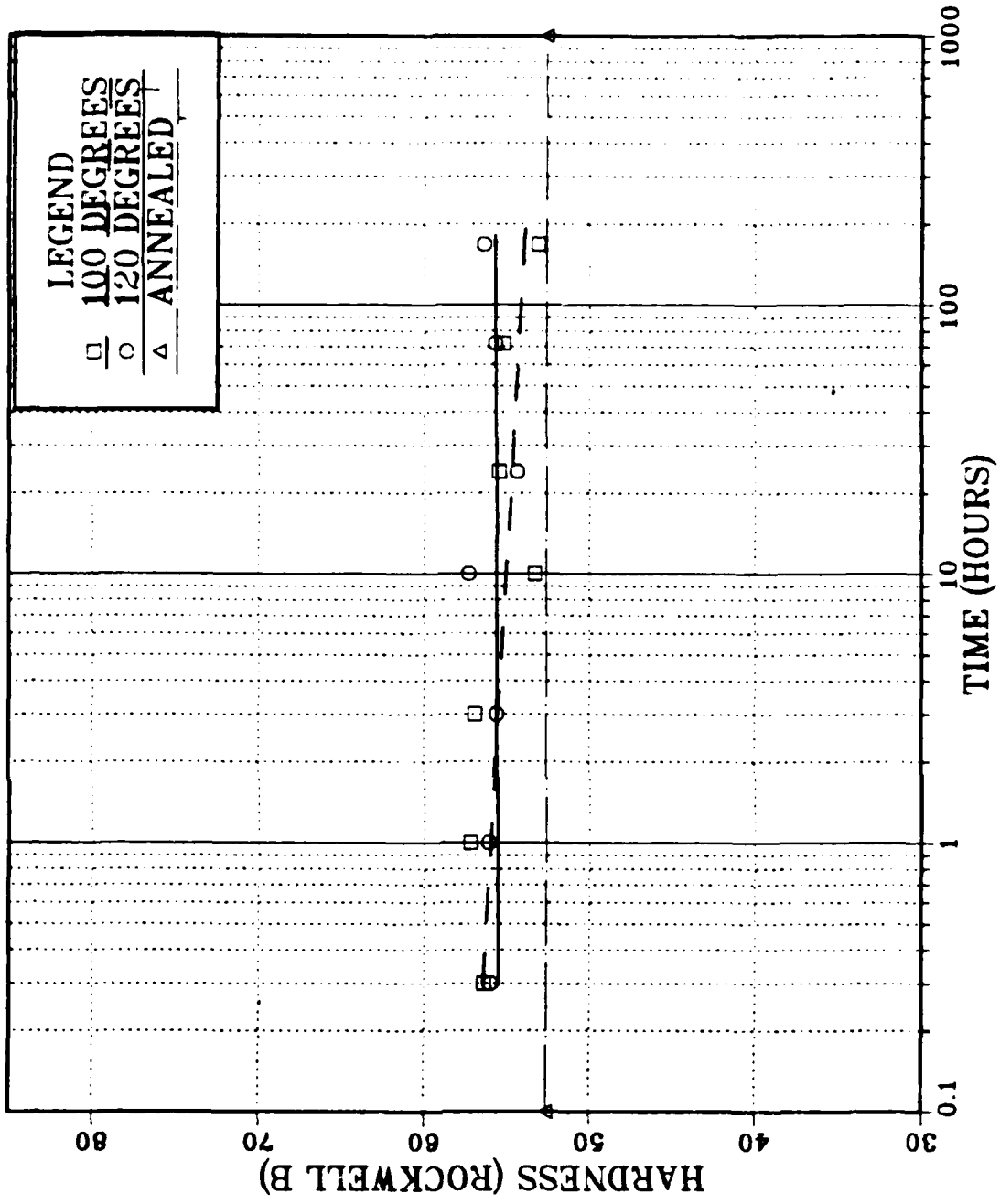

Figure 4.2 Age Hardening Response of the 8%Mg-1%Li Alloy

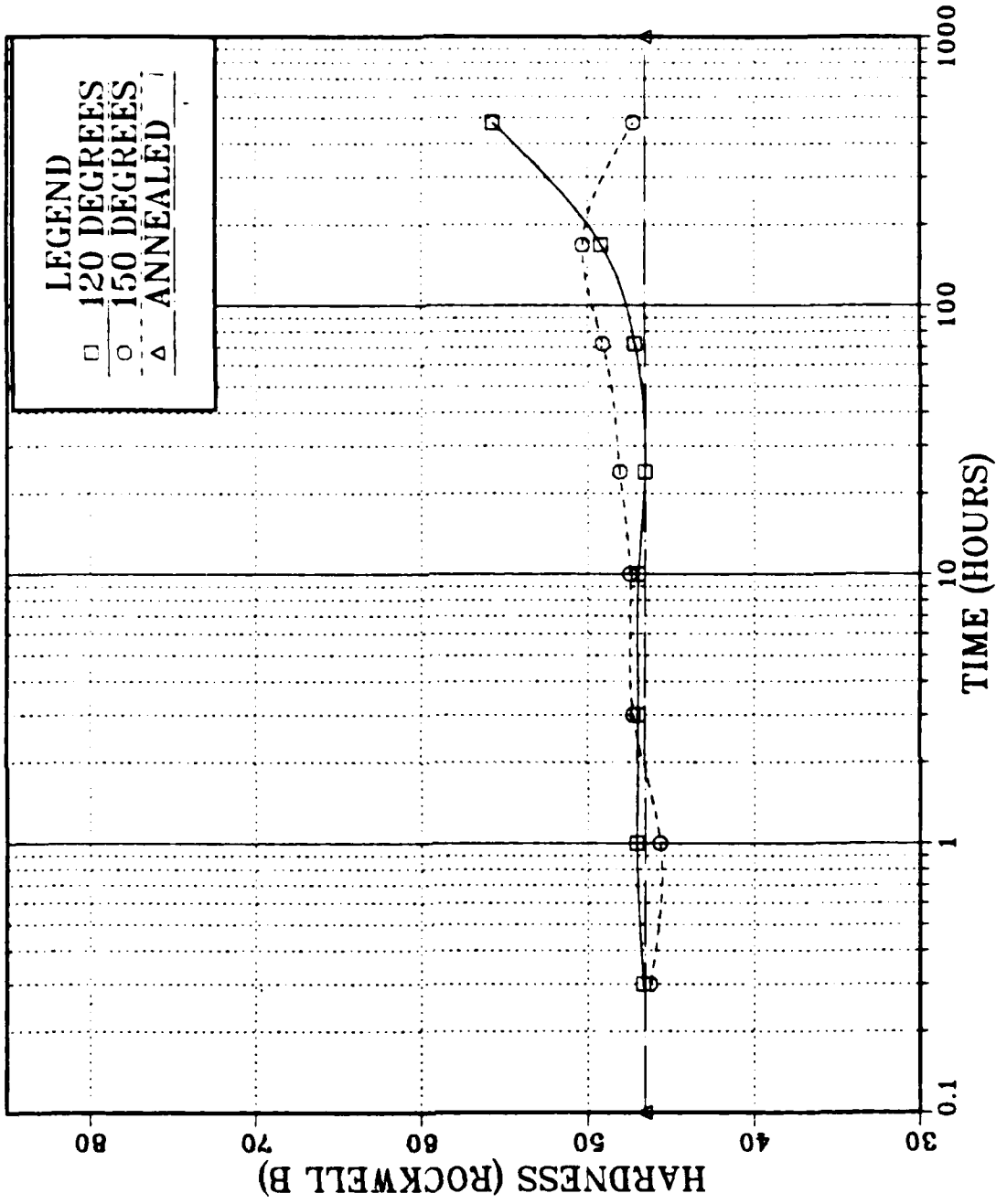

Figure 4.3 Age Hardening Response of the 6%Mg-1%Li Alloy

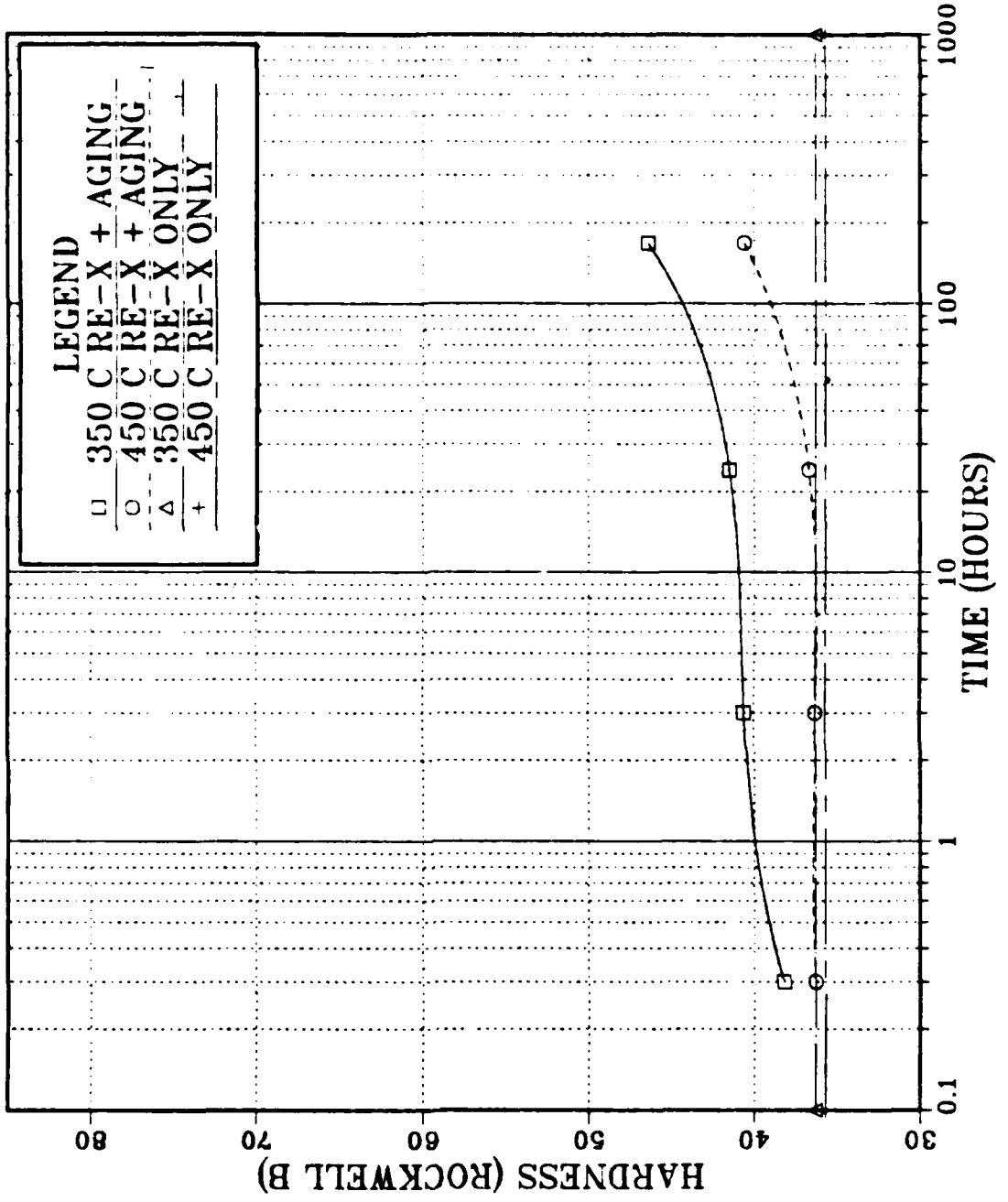

Figure 4.4 Age Hardening Response of the Recrystallized 6%Mg-1%Li Alloy

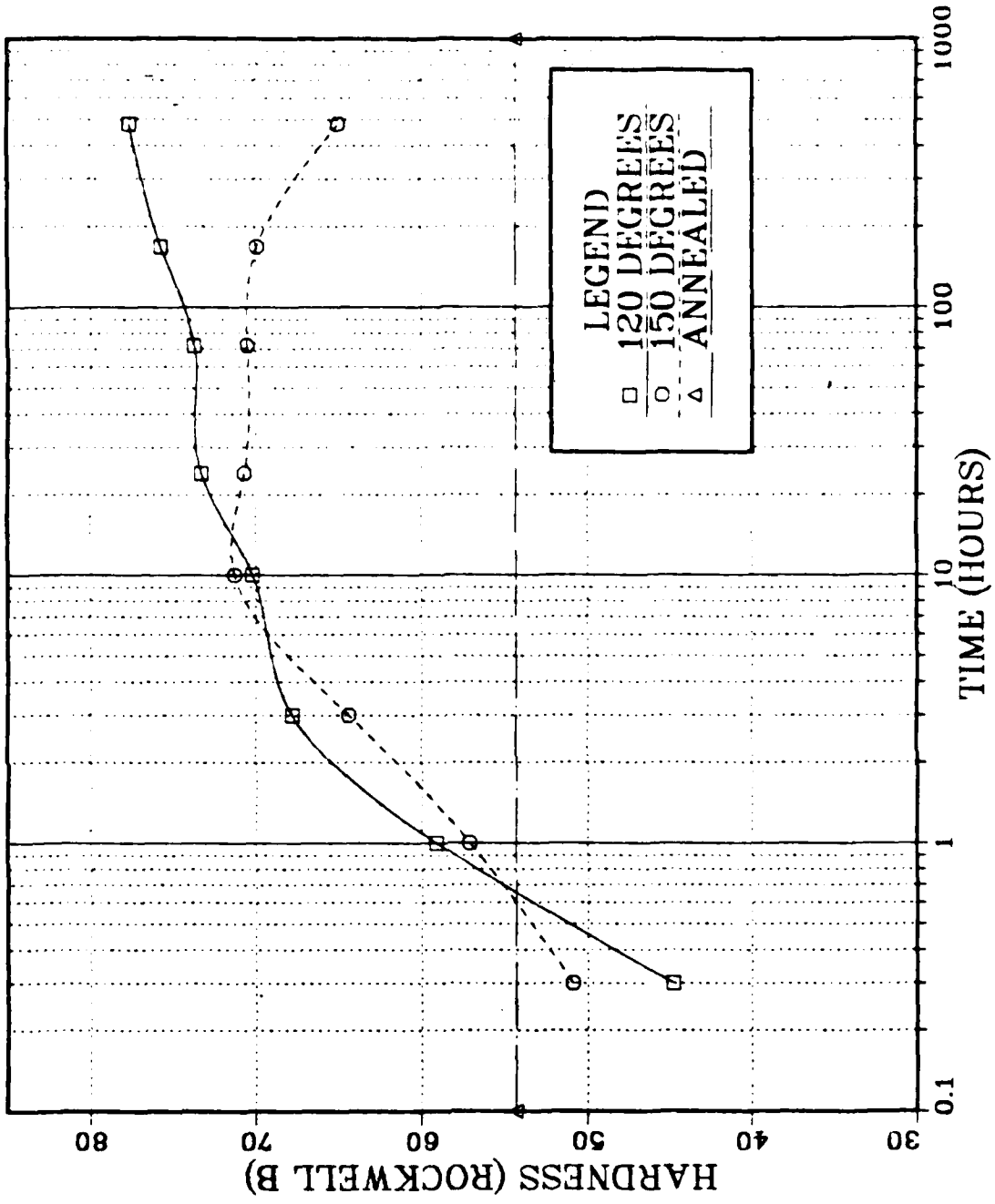

Figure 4.5 Age Hardening Response of the 6%Mg-2%Li Alloy

120 C curve, while the latter was still going up at 480 hours. Both alloys showed initial softening, but had a noticeable hardening by 1 hour, with the 120 C curve showing the faster response. The difference between the hardnesses of the two curves at the 1 and 3 hour points are within twice the estimated data scatter.

B. TRANSMISSION ELECTRON MICROSCOPY DATA

1. 8%Mg-1%Li

a. Annealed

TEM investigation of the 8%Mg-1%Li alloy in the annealed condition revealed a fine microstructure with several distinct types of regions. In a few areas, some dislocation networks were visible; however, recovered regions, characterized by low-angle boundaries, and subgrains of 1-3 μm size were more prevalent (Figure 4.6). Another type of region found appeared to be continuously recrystallized, which has a clean microstructure, relatively free of dislocations, and with moderate-angle boundaries (Figure 4.7). Grains are generally smaller than 5 μm; grain growth has not occurred. Another type of region appears to have undergone continuous recrystallization and grain growth, or possibly discontinuous recrystallization and grain growth (Figure 4.8). Here, some large grains of 20 μm in size are present.

Second phases present include fairly homogeneously distributed 0.5-1 μm size β. Also found are cuboidal appearing primary Al_3Zr, and an inhomogeneous distribution of spheroidal secondary Al_3Zr of about 10 nm size. Also present are irregularly shaped particles which were unidentifiable by the selected area diffraction pattern (SADP) technique used to identify the other phases.

Second phases, particularly β, appeared to retard coarsening of the microstructure. β-rich areas were considerably finer than the β-lean areas. A mechanism for this can be seen in Figure 4.8, where a large grain's boundary is being forced to bow around β particles as it attempts to grow (upward in the micrograph) into a region of finer microstructure, and greater β density. Areas high in secondary Al_3Zr content also appeared to have a finer microstructure.

b. Aged at 120°C for 168 hours

The aged microstructure is remarkably similar to the annealed microstructure. The same types of regions, recovered (Figure 4.9), continuously recrystallized (Figure 4.10), and discontinuously recrystallized (Figure 4.11), and the same second phases were found. No δ′ appeared in diffraction patterns. Neither grains nor second phase particles have undergone significant growth, indicating a stable microstructure.

Figure 4.6 Al-Mg-Li Annealed, Recovered Region

Refined sub grain structure and reduced dislocation density are evident in (a), with (b) being a higher magnification.

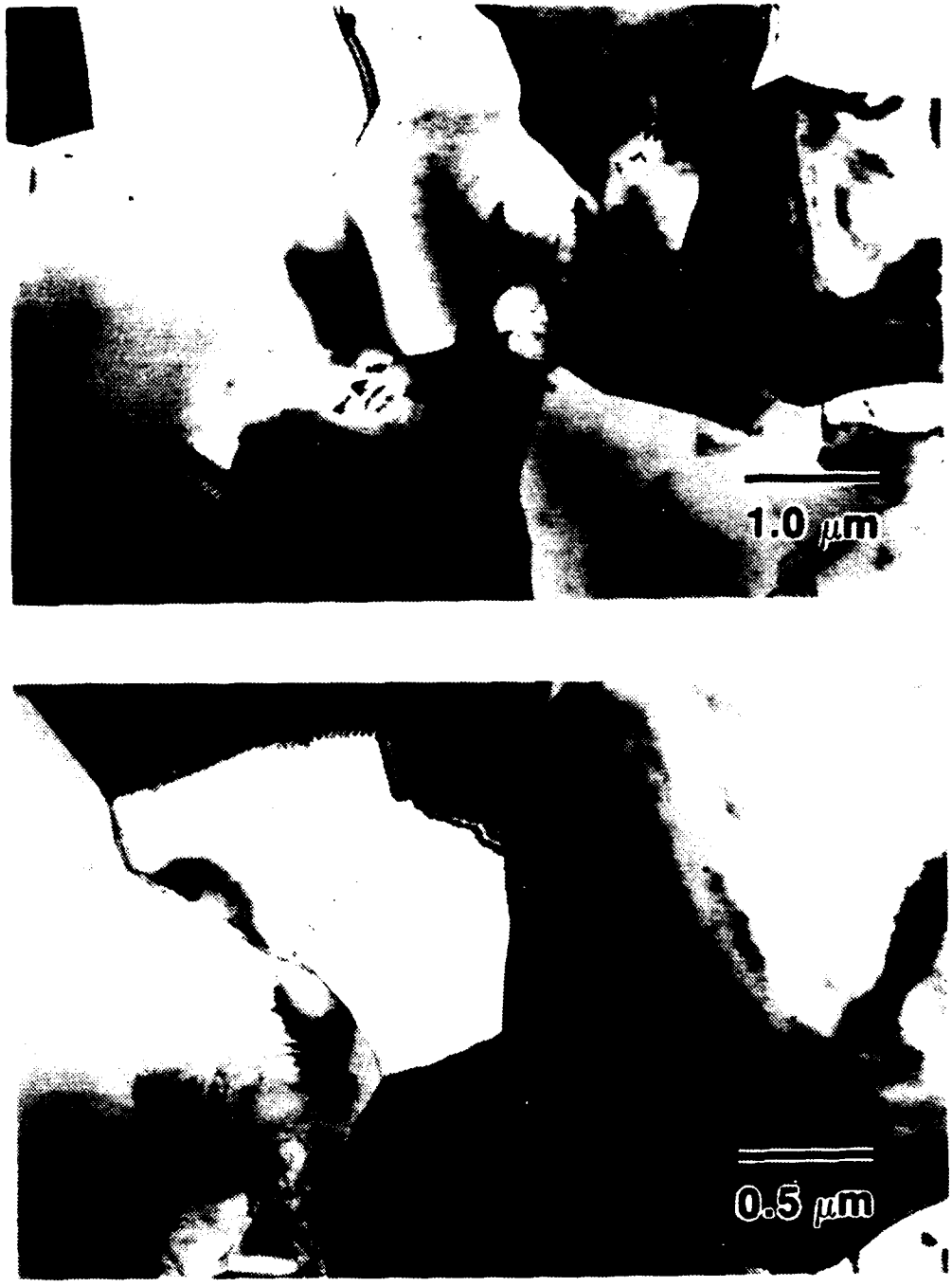

Figure 4.7 5% Mg-1%Li Annealed, Continuously Recrystallized (CRX) Region

Strain free grains, moderate-angle boundaries, and "clean" microstructure are apparent. Dislocations at the moderate-angle boundaries are more apparent in (b).

Figure 4.8 8%Mg-1%Li Annealed,
Discontinuously Recrystallized (DRX) Region

Note the large grain at the bottom of (a) growing upward into an area of finer structure. The β particles appear to be retarding boundary migration by Zener drag, as shown in the higher magnification of (b).

Figure 4.9 8% Mg-1% Li Aged at 120°C for 168 Hours, Recovered Region

Micrograph (a) is a recovered region with (b) showing moderate dislocation density remaining.

2. **6%Mg-1%Li**

a. Annealed

The annealed 6%Mg-1%Li microstructure is similar to the annealed 8%Mg-1%Li. Figure 4.12 is representative of an area that is mostly recovered, but still shows some dislocation networks. This is substantially more organized than the dense dislocation tangles found by Munro [Ref. 34] in his TEM investigation of this alloy in the as-rolled condition. Subgrains are fine, averaging 2-3 μm. Figure 4.13 is a bright field-dark field pair of a recovered region with retained dislocation arrays. Figure 4.14 shows the boundary between a large recrystallized grain and an area of finer microstructure that has not undergone discontinuous recrystallization. TEM examination of this alloy revealed more primary Al_3Zr than was found in the 8%Mg-1%Li alloy, due to the almost double concentration of Zr.

b. Aged 120°C for 168 hours

TEM reinforces the parallel between this alloy and the 8%Mg-1%Li alloy. The same types of microstructural regions and second phases are present. Diffraction patterns revealed no δ′. Figure 4.15 shows a region that is in the early stages of recovery, with considerable dislocation density. Areas like this were also found in the 8%Mg-1%Li alloy. Dislocations were more prevalent in areas without β, indicating that β aids in recovery. Figure 4.16 is of a recrystallized region of mostly strain free grains with well defined moderate and high angle boundaries. Figure 4.17 depicts a recrystallized grain with a distribution of roughly spheroidal secondary Al_3Zr. Figure 4.18 is a bright field-dark field pair of the interior of a large recrystallized grain showing a β particle, secondary Al_3Zr particles pinning some of the remaining dislocations, and a low angle boundary within the grain. Figure 4.19 is a spheroidal, faulted β particle with its unmistakable constellation SADP.

As with the 8%Mg-1%Li alloy, the microstructure of the 6%Mg-1%Li showed little change in either the matrix or the second phases on aging. Similarly, no δ′ was found.

(a)

(b)

Figure 4.10 8%Mg-1%Li Aged at 120 C for 168 Hours, CRX Region

Fine, continuously recrystallized region with moderate volume fraction of sub-micron sized β evident in (a). In (b), details such as the spheroidal secondary (2°) Al_3Zr and irregularly shaped unidentified particles are more visible.

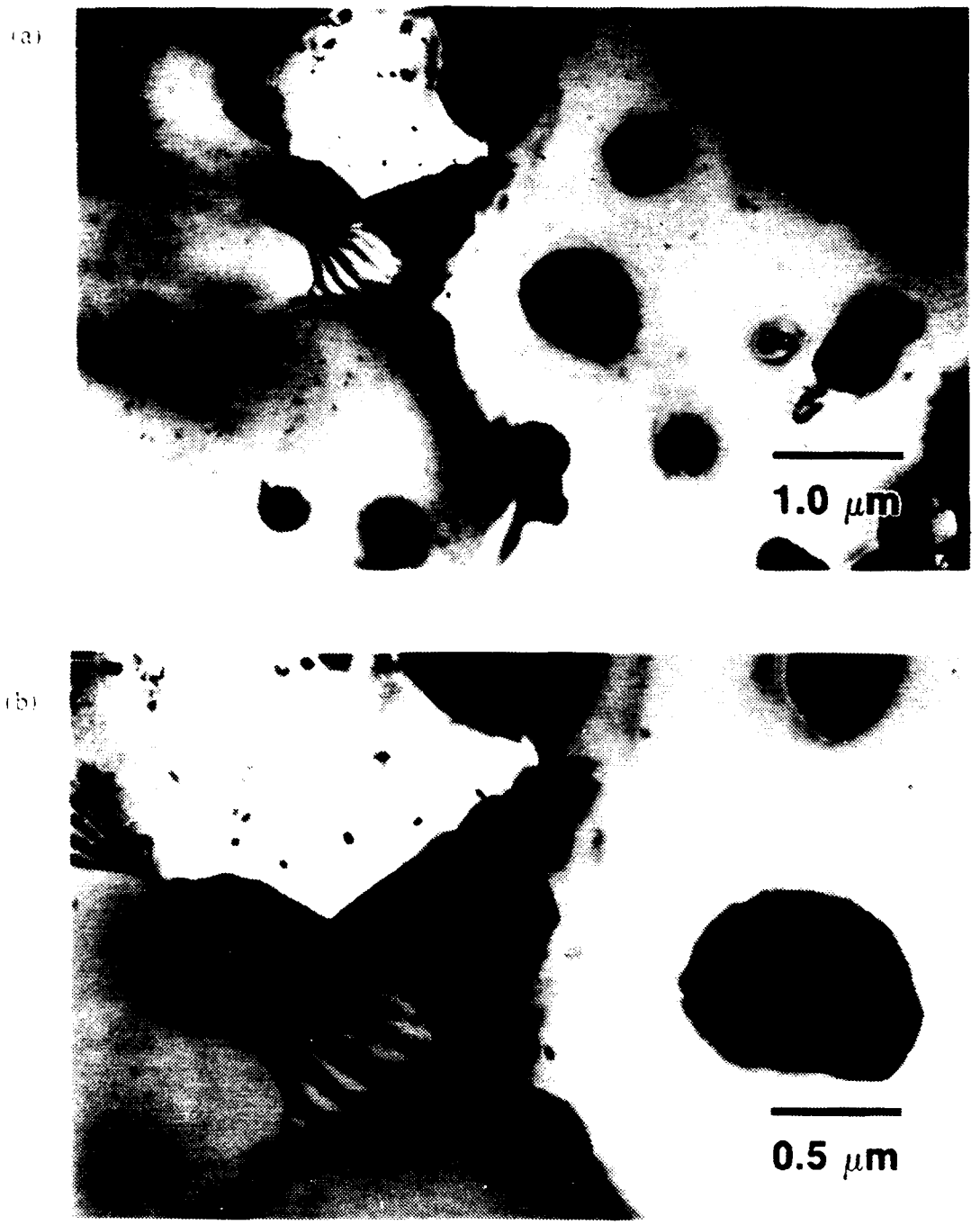

Figure 4.11 8%Mg-1%Li Aged at 120°C for 168 Hours, DRX Region

On the right is a large discontinuously recrystallized grain containing a higher volume fraction of β than is typical of such grains. A higher magnification detail, (b), shows β particles on the boundary.

Figure 4.12 6%Mg-1%Li Annealed, Dislocation Substructure

A recovering region with moderate dislocation substructure remaining. Micrograph (b) is a higher magnification of (a), showing dislocations in arrays, rather than the dense tangles found in the as-rolled condition.

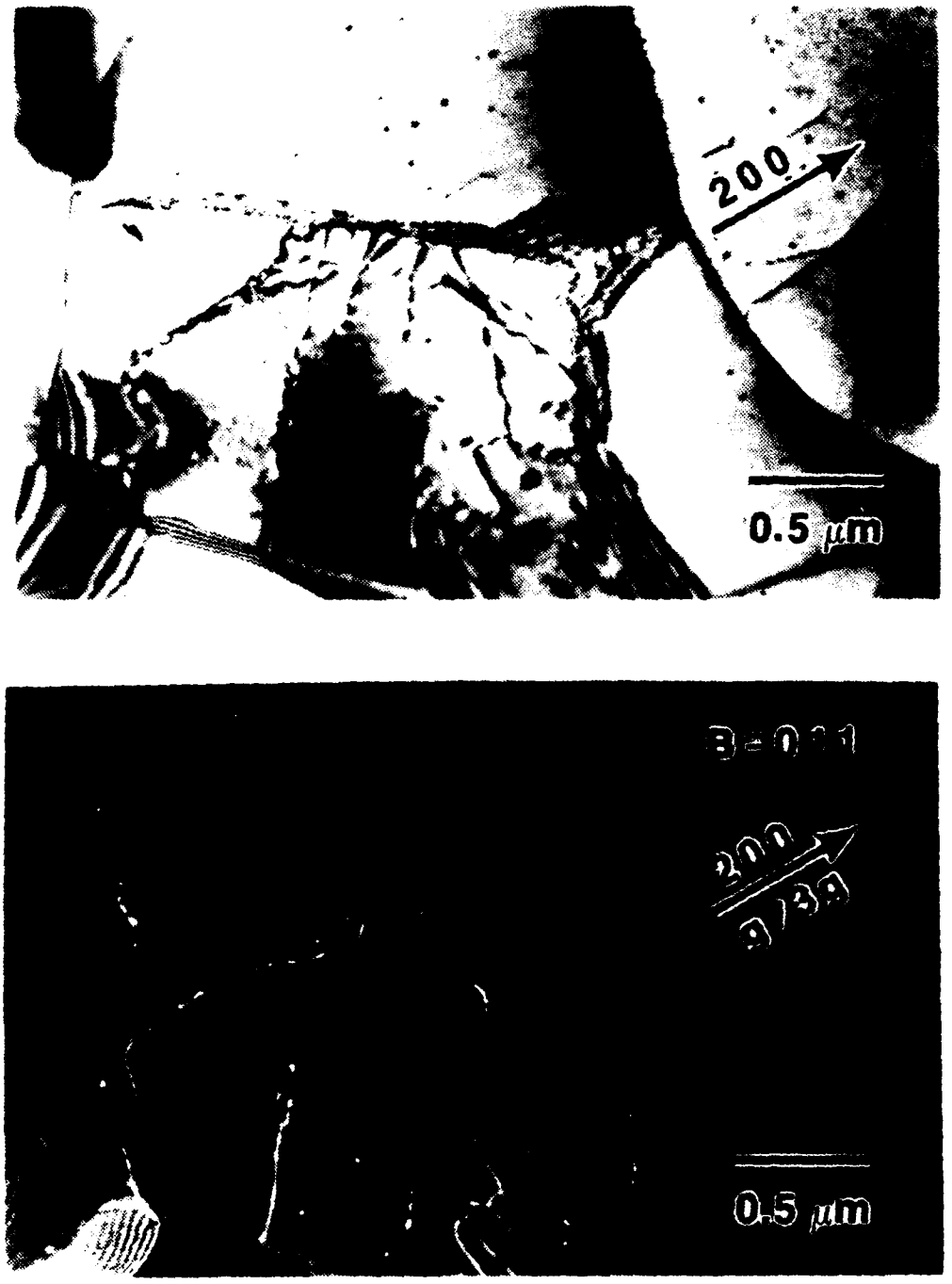

Figure 4.13 6%Mg-1%Li Annealed, Dislocation Arrays

BF(a) WBDF(b) pair of recovered microstructure showing arrayed nature of remaining dislocations, and highlighting dislocation nature of the boundaries.

(a)

(b)

Figure 4.14 6%Mg-1%Li Annealed, DRX Grain

Discontinuously recrystallized large grain on the left, in (a), and a finer, recovered substructure on the right. In (b), a higher magnification detail of (a), the β particles and the boundary are more apparent.

(a)

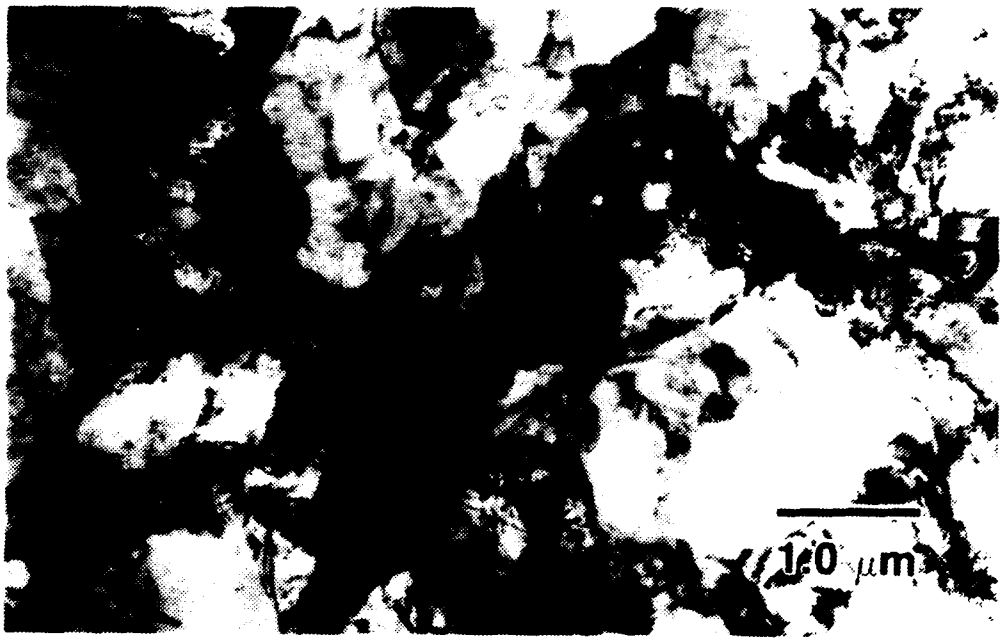

(b)

Figure 4.15 6% Mg-1% Li Aged at 120 C for 168 Hours, Dislocations

Region in early stages of recovery, showing a considerable amount of unorganized dislocation substructure remaining. In (a), note the absence of β. Micrograph (b) details the high dislocation density.

Figure 4.16 6%Mg-1%Li Aged at 120°C for 168 Hours, CRX Region

Fine, continuously recrystallized region with moderate- and high-angle grain boundaries. In (b), grain boundaries are more visible than in the lower magnification (a).

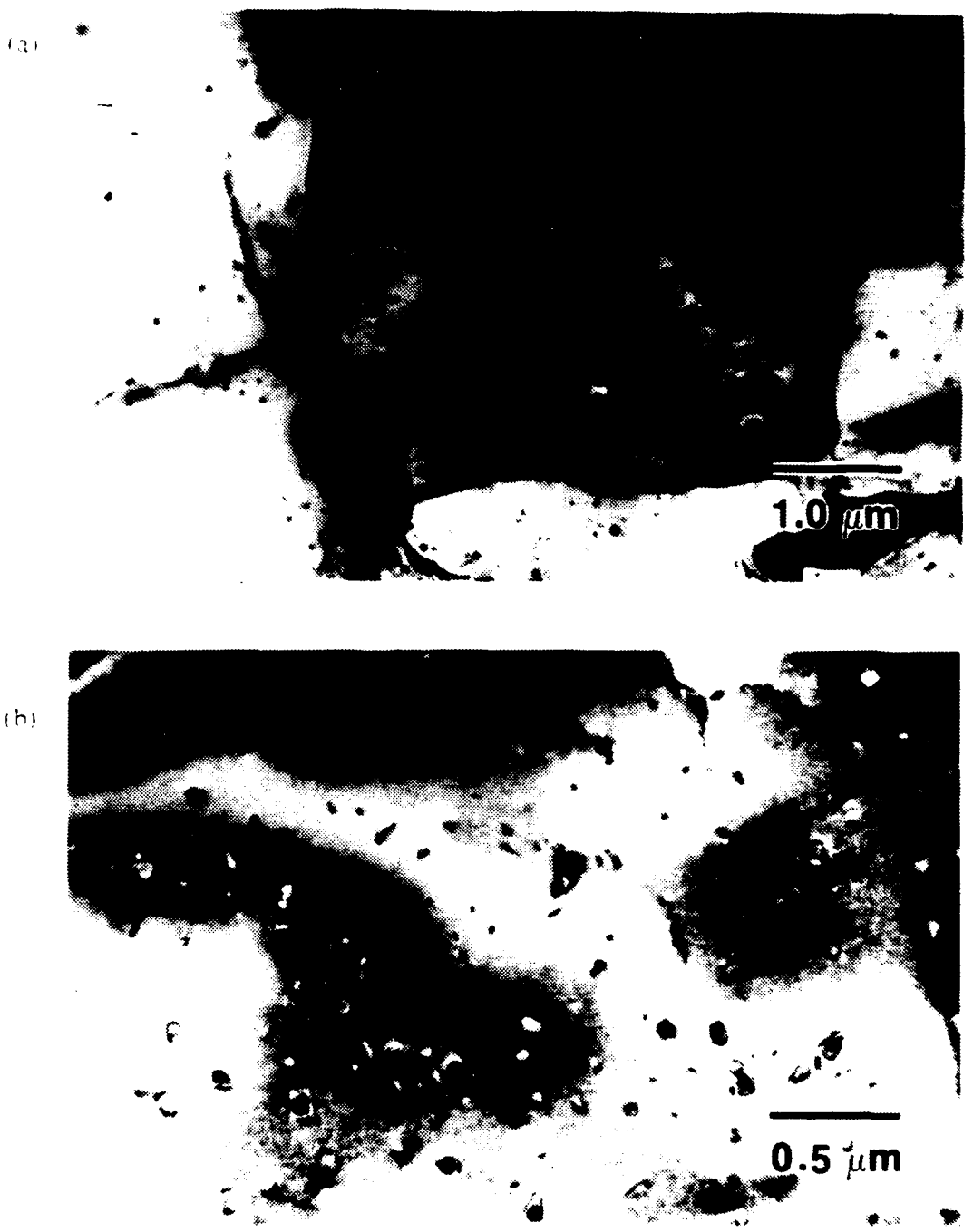

Figure 4.17 6%Mg-1%Li Aged at 120°C for 168 Hours, 2° Al_3Zr

Moderate sized recrystallized grain (a) with distribution of roughly spheroidal, 25-75 nm, secondary Al_3Zr more evident in the higher magnification of (b).

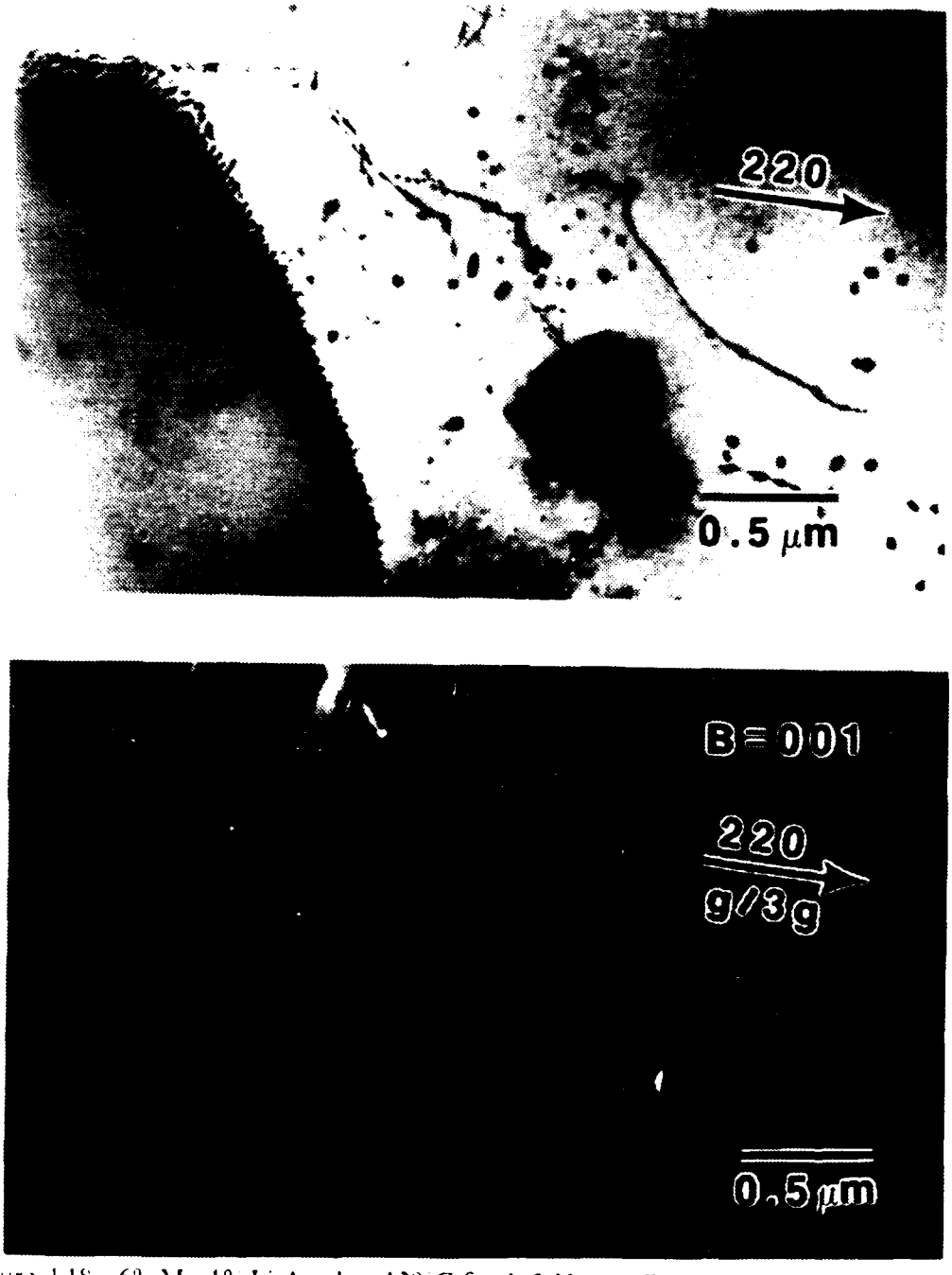

Figure 4.18 6%Mg-1%Li Aged at 120°C for 168 Hours, Dislocation Arrays

Boundary dislocation arrays are a striking feature of this BF(a) WBDF(b) pair of a large recrystallized grain with a distribution of spheroidal secondary Al_3Zr and a β particles. Al_3Zr particles are smaller (20-50 nm) and more uniform than in Figure 4.17. In b, strain fields around particles are evident.

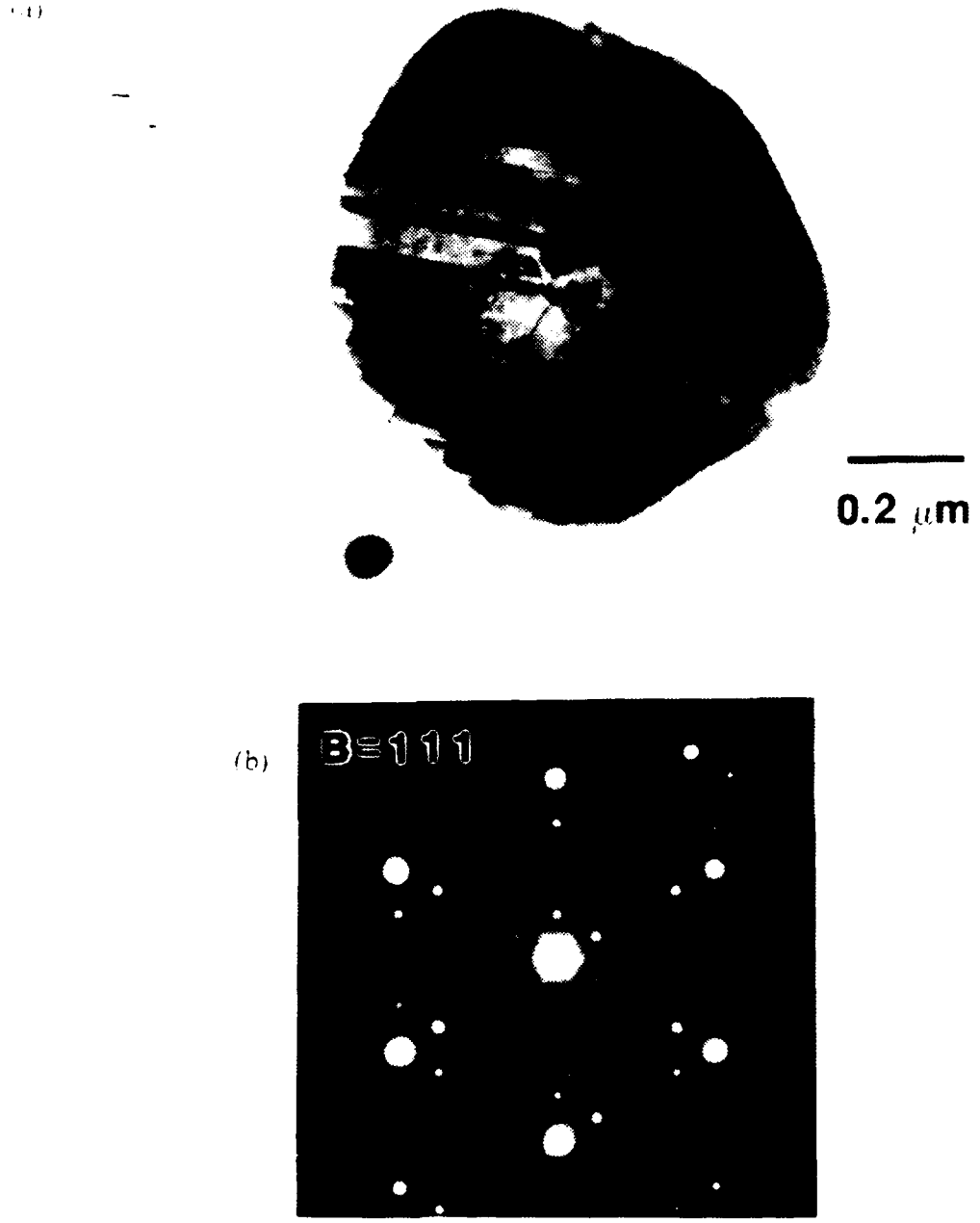

Figure 4.19 6%Mg-1%Li Aged at 120°C for 168 Hours, β particle

Heavily faulted, roughly spheroidal, β particle, of typical submicron size, (a), with its characteristic, closely spaced constellation SADP in (b).

3. 6%Mg-2%Li

Serious difficulties were encountered in rolling this alloy. Rolling was attempted at 300°C, 350°C, and 375°C, with all billets suffering edge cracking and alligatoring. Optical microscopy revealed some grain boundary decoration, but was not conclusive of intergranular cracking.

a. Annealed

The microstructure of the annealed 6%Mg-2%Li alloy has many similarities to the previously discussed alloys. Figures 4.20 and 4.21 are illustrative of the subgrain structure typical of all the alloys studied. Figure 4.20 clearly shows thickness fringes at a boundary. Figure 4.21 shows the dislocation arrays at the low-angle boundaries characteristic to the regions of substructure. Figure 4.22 displays one of the points of departure of this alloy from the lower lithium compositions. On the right are the spheroidal secondary Al_3Zr particles common to all the alloys, but on the left are larger, more irregularly shaped particles that were identified by SADP to be Al_2MgLi. This is the first evidence that the 6%Mg-2%Li may be expected to behave as a true ternary alloy, rather than as a quasi-binary Al-Mg alloy. The inhomogeneity of the secondary Al_3Zr is also evident, with the left side of the micrograph almost devoid of it. Figure 4.23 further explores the Al_3Zr in a bright-field dark-field pair. On the right, the particles are smaller (about 20 nm), but constitute a larger volume fraction than on the left, where the particles are 40 to 50 nm in size.

b. Aged 120°C for 10 hours

There are many similarities between microstructures of the aged 6%Mg-2%Li alloy and the lower lithium alloys; Figure 4.24 highlights a major difference. A homogeneous dispersion of fine (about 3 nm), spheroidal δ' is evident throughout the micrograph. Not pictured, but found in several TEM specimens of the 6%Mg-2%Li alloy of different thermal histories, were irregularly shaped precipitates that could not be identified by either SADP or morphology. They were suspected of being $Al_{12}(Mg,Li)_{17}$, which is predicted by the phase diagram.

c. Aged 150°C for 10 Hours

Figures 4.25 and 4.26 point out the similarities of this condition to previously studied ones. Figure 4.25 is an area of fine substructure with low-angle boundaries. Figure 4.26 is an example of a high-angle boundary separating two strain free recrystallized grains. Figure 4.27 spotlights another significant difference between the higher and lower lithium containing alloys, Al_2MgLi. Figure 4.28 points up a

(a)

(b)

Figure 4.20 6%Mg-2%Li Annealed, Recovered Region

Thickness fringes on the boundary are notably visible in this pair of different magnification micrographs of the same grain. The dislocation array in the grain interior is visible at the upper right corner of (b).

(a)

(b)

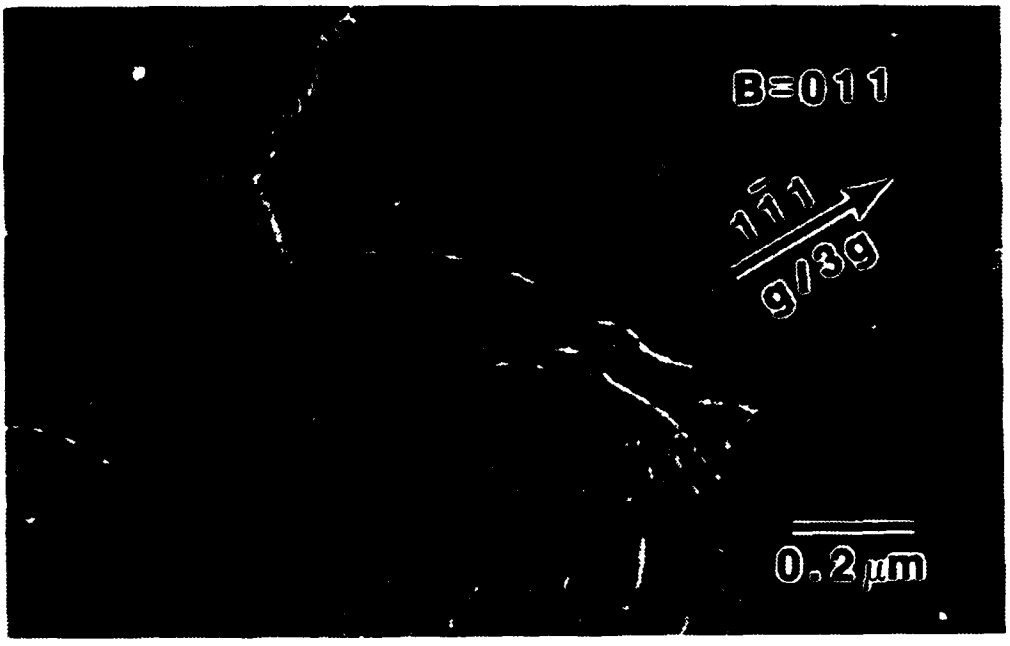

Figure 4.21 6°-Mg-2°-Li Annealed, Dislocation Arrays

An inhomogeneous distribution of 10-20 nm sized secondary Al_3Zr and dislocation arrays are visible in this BF(a) DF(b) pair.

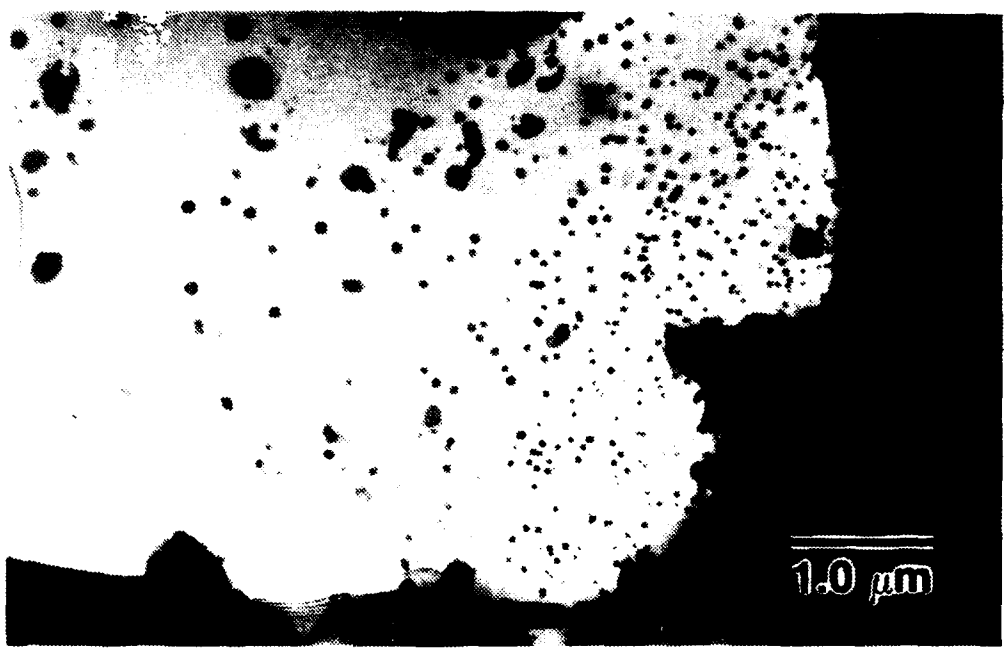

Figure 4.22 6%Mg-2%Li Annealed,
Secondary Al_3Zr and Al_2MgLi

Inhomogeneous distributions of spheroidal secondary Al_3Zr and irregularly shaped Al_2MgLi are visible in this micrograph.

(a)

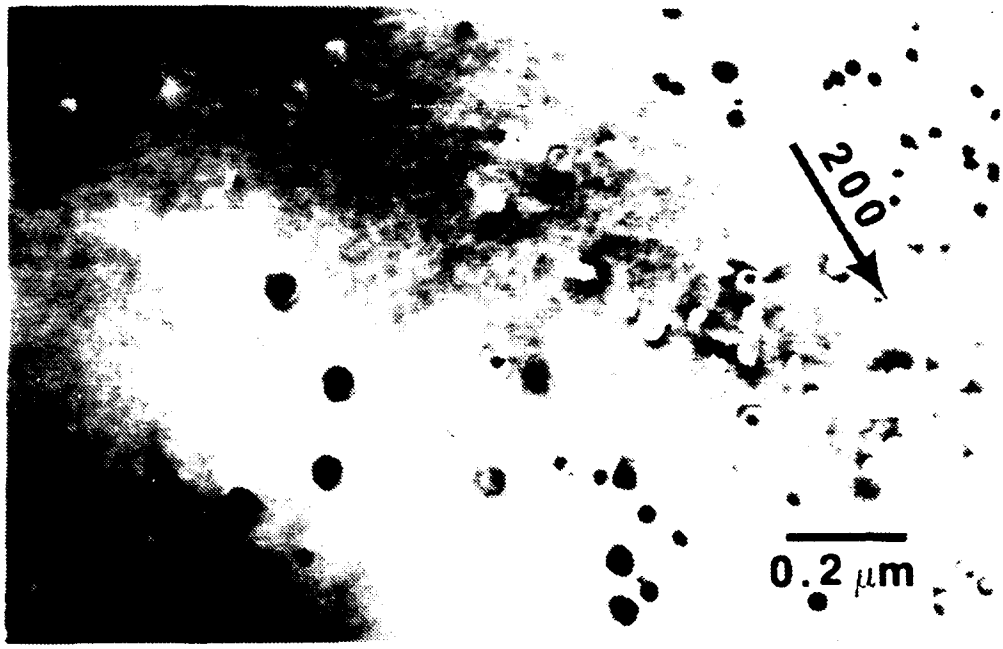

(b)

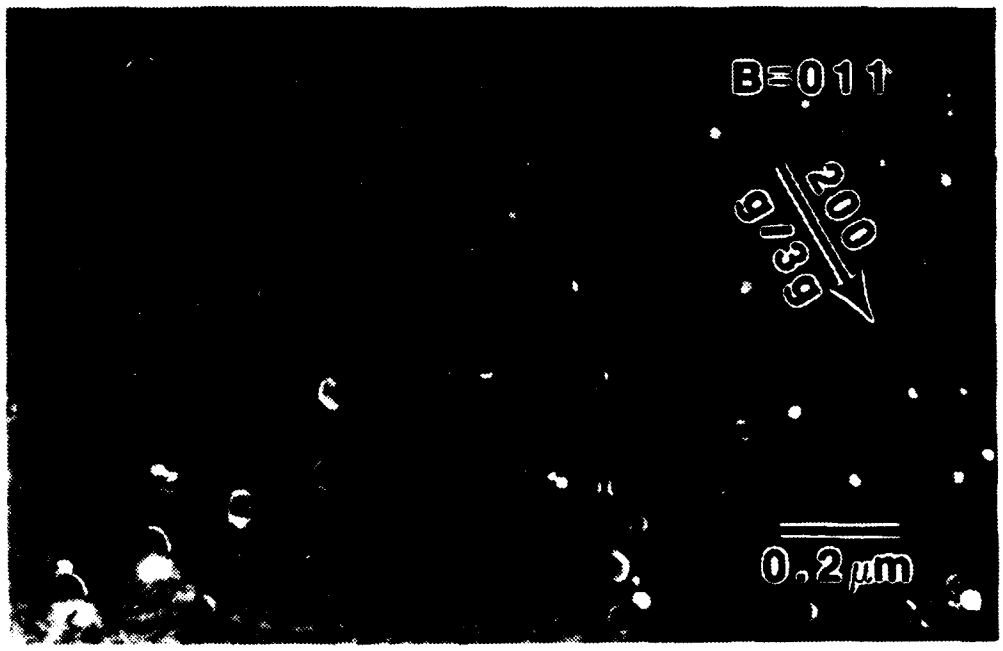

Figure 4.23 6%Mg-2%Li Annealed, Inhomogeneous Al_3Zr

This BF(a) WBDF(b) micrograph pair displays the inhomogeneities in size and volume fraction of the distribution of secondary Al_3Zr. Particles range in size from 10 to 75 nm.

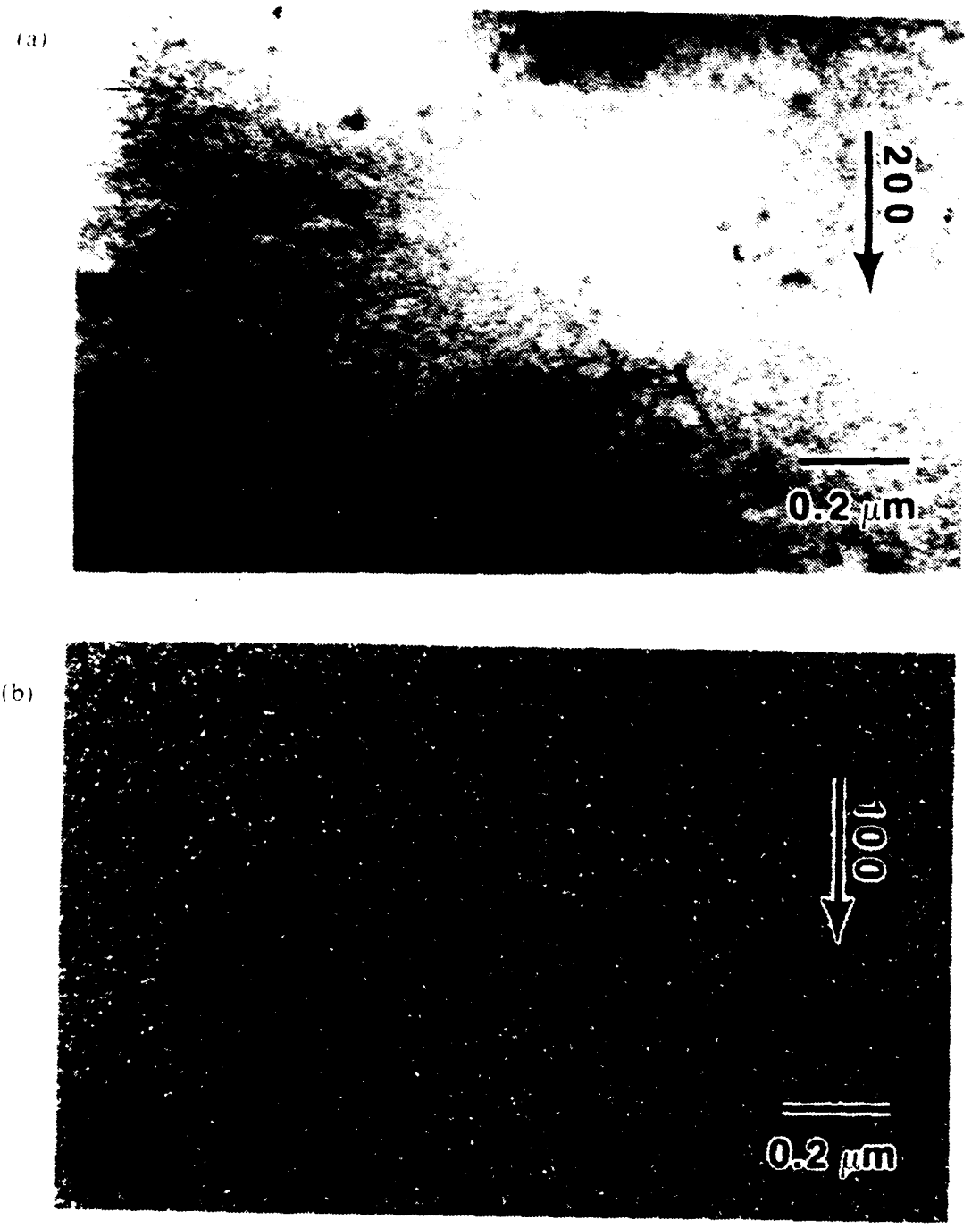

Figure 4.24 6%Mg-2%Li Aged 120°C for 10 Hours, Homogeneous δ'

BF(a) DF(b) pair of fine (6-12 nm), and uniformly distributed δ'.

difference in the δ′ between specimens aged at 120°C and 150°C; the higher temperature produced precipitates that appear to be at least twice the size, and have slightly greater spacing, than the lower temperature. The hardness data are indistinguishably different. Figure 4.29 shows the complete absence of a PFZ at a high-angle boundary, and is also representative of the lack of significant grain boundary precipitation.

d. Aged 120°C for 168 hours

Even after 168 hours at temperature, 6%Mg-2%Li, like the other alloys, has recovered regions, with some dislocation substructure and low-angle boundaries (Figure 4.30). Figure 4.31 is a SADP and the area from which it came, showing the superlattice reflections used to identify δ′. Figure 4.32 shows that some coarsening of the δ has occurred (to about 10 nm), but it is still homogeneously distributed, with no PFZ's found. The volume fraction of δ′ has increased to an estimated 1.3. Figure 4.33 is bright-field dark-field pair showing that zirconium additions can bring about strengthening, too. In this region, where secondary Al_3Zr is finer (about 15 nm), and more homogeneously distributed than is typical, precipitates can be seen interacting with dislocations across the center of the micrograph. Figure 4.34 depicts a feature common to all the alloys in all the conditions examined. It is a part of a large (greater than 7 μm), cuboidal primary Al_3Zr particle, and its diffraction pattern.

(a)

(b)

Figure 4.25 6%Mg-2%Li Aged 150°C for 10 Hours, Fine Substructure

This micrograph pair is representative of the regions of fine substructure and low-angle boundaries. Micrograph (b) is a higher magnification detail of (a).

Figure 4.26 6%Mg-2%Li Aged 150°C for 10 Hours.
High-Angle Grain Boundary

Visible are the larger Al_2MgLi particles and the smaller secondary Al_3Zr. This grain boundary is representative of the relative freedom from preferential grain boundary precipitation found.

(a)

(b)

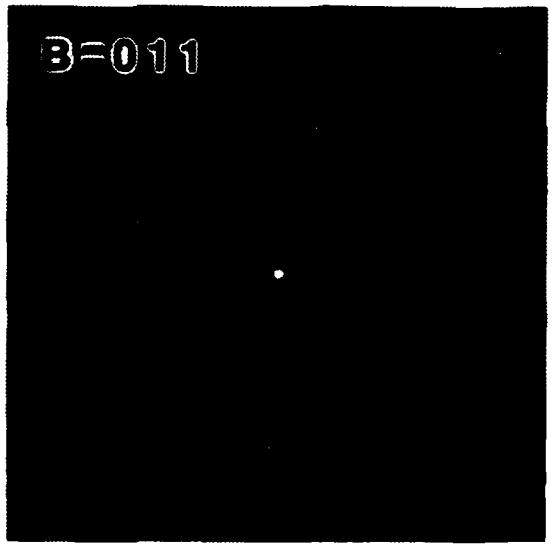

Figure 4.27 6%Mg-2%Li Aged 150°C for 10 Hours, Al_2MgLi

In (a), two elongated Al_2MgLi particles, and (b), a zone axis SADP from one confirming identification.

(a)

(b)

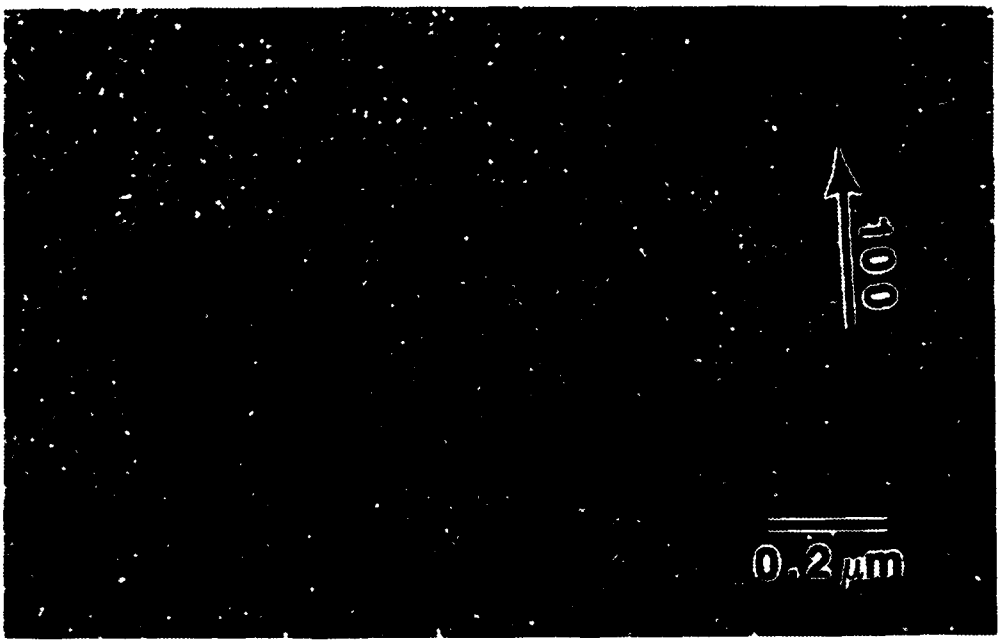

Figure 4.28 6% Mg-2% Li Aged 150°C for 10 Hours, Homogeneous δ'

BF(a) DF(b) pair showing secondary Al_3Zr, and the more coarse δ' than that of the 120°C aging condition of Figure 4.24.

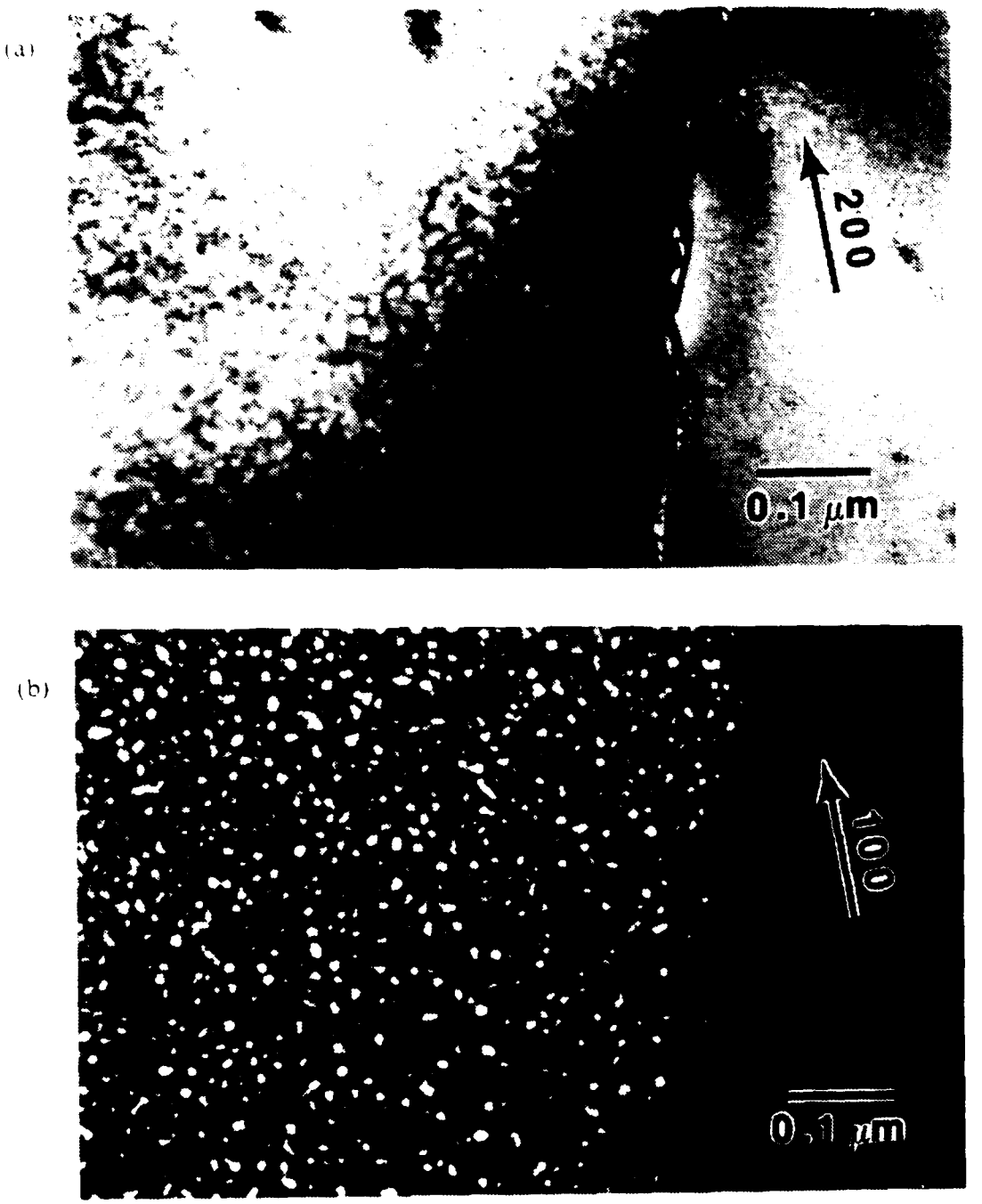

Figure 4.29 6% Mg-2% Li Aged 150°C for 10 Hours.
High-Angle Grain Boundary With No PFZ

BF (a) DF (b) pair showing the homogeneous distribution and high volume fraction of δ'. Noteworthy are the complete lack of a PFZ, and the absence of significant grain boundary decoration.

Figure 4.30 6%Mg-2%Li Aged 120 C for 168 Hours, Early Stages of Recovery

Like the other alloys, even after extended heat treatment, the 6%Mg-2%Li alloy had regions of recovered microstructure.

(a)

(b)

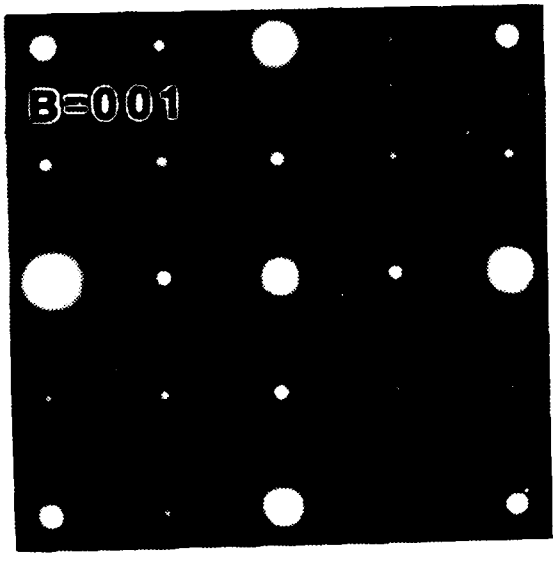

Figure 4.31 6%Mg-2%Li Aged 120°C for 168 Hours,
δ' Superlattice SADP

Grain boundary between two recrystallized grains (a), and a SADP (b) of the region showing the superlattice reflections used to identify the δ' present, but not imaged in this micrograph.

(a)

(b)

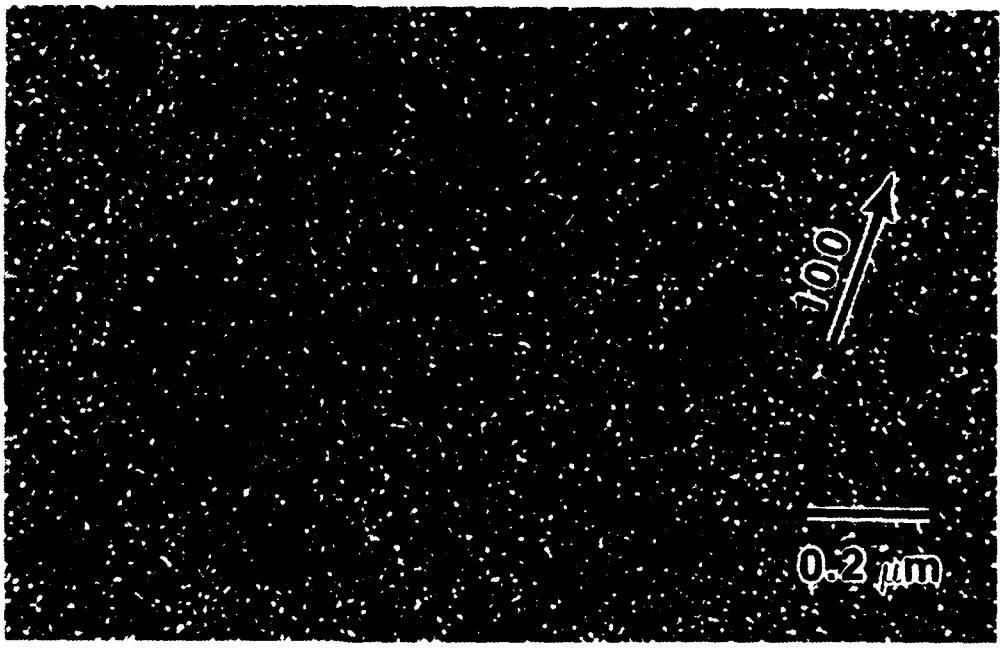

Figure 4.32 6%Mg-2%Li Aged 120°C for 168 Hours, Coarsening δ'

The coarsening of the δ' over time is evident when comparing this BF(a) DF(b) pair of micrographs to Figure 4.24. The δ' volume fraction is estimated to be about 1.3.

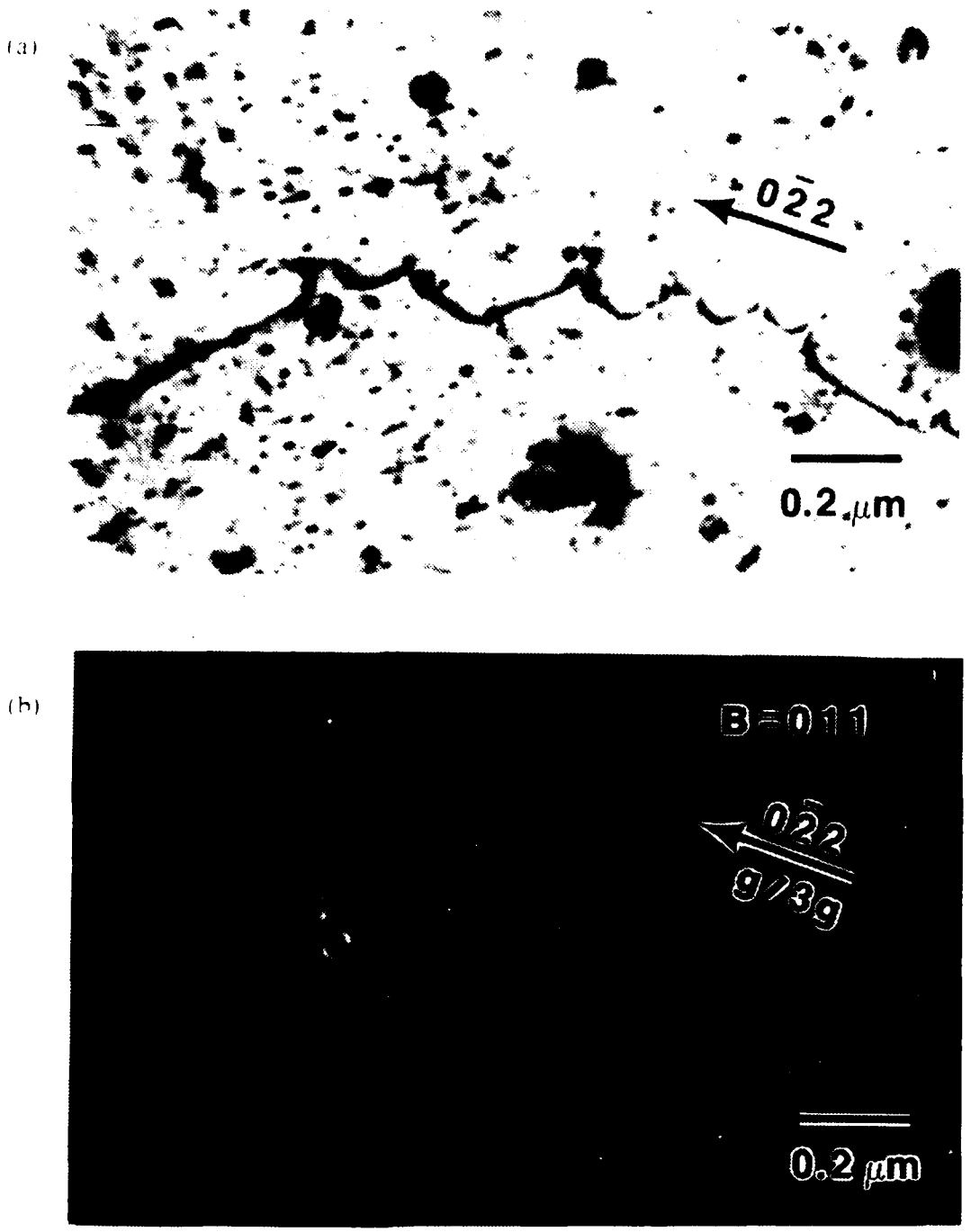

Figure 4.33 6%Mg-2%Li Aged 120°C for 168 Hours, Secondary Al_3Zr Pinning Dislocations

An additional source of strengthening in this alloy system is provided by the secondary Al_3Zr, which in this BF(a) WBDF(b) pair is shown forcing dislocations to bow.

(a)

(b)

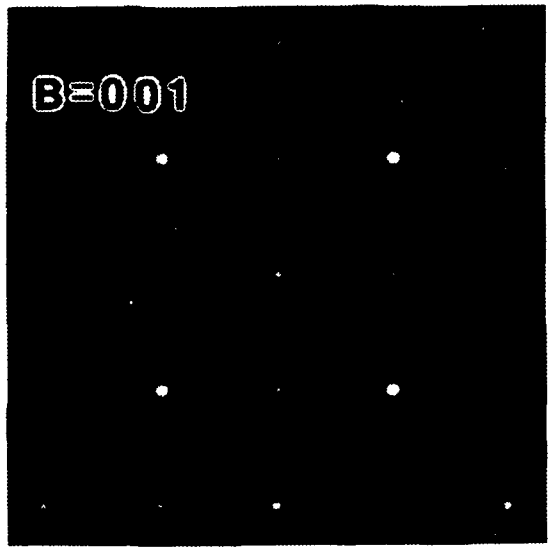

Figure 4.34 6%Mg-2%Li Aged 120°C for 168 Hours, Primary Al_3Zr and SADP

Depicted in (a) is the corner of a large (about 7 μm) primary Al_3Zr particle and the SADP (b) used to identify it.

C. SUMMARY OF RESULTS

1. Only the 6%Mg-2%Li alloy precipitated δ', and was the only alloy to show a significant age hardening response.
2. The 6%Mg-1%Li alloy showed a slight hardening response after long aging that was not due to δ' precipitation.
3. All alloys had regions in various stages of recovery, regions that had been recrystallized, and regions in which a few grains had undergone grain growth.
4. The microstructure and second phases (with the exception of δ' in the 6%Mg-2%Li) of all alloys showed no significant changes on aging.
5. The 1%Li alloys precipitated β, but no ternary phases.
6. The precipitation of Al_2MgLi was verified in the 6%Mg-2%Li alloy; $Al_{12}(Mg,Li)_{17}$ was suspected, and no β was seen.

V. DISCUSSION

A. MICROSTRUCTURE

The TMP used at NPS is designed to produce a fine substructure which will undergo continuous recrystallization preceding and concurrent with deformation, producing a fine and stable structure of moderate- and high-angle boundaries capable of sustaining SPD. Rolling is done below the β solvus to allow β precipitation on dislocations [Ref. 19]. Continued rolling homogenizes the microstructure, producing a fairly even distribution of β, which refines the grain structure resulting from continuous recrystallization [Ref. 20]. This processing, in the alloys studied in this research, produced microstructures capable of elongations in excess 1000%, at relatively low temperature ($0.7T_m$) and high strain rates (10^{-3} to 10^{-2} per second) [Ref. 35].

It should be noted that the microstructure of the coupons and that of the undeformed grip sections of SPD tensile specimens may not be directly comparable due to the vastly different heating rates they experience. The coupons come to temperature within a few seconds of being placed in a hot furnace. On the other hand, the tensile specimens are placed in room temperature grips, which are then placed in a hot furnace. It is estimated that heating rates differ by as much as three orders of magnitude.

In the course of the TEM investigation, it was noted that a significant area fraction of the foils exhibited a recovered substructure as well as a fine grain structure. Previous research at NPS concluded continuous recrystallization to be the dominant transformation mode during heating. The mixed microstructure seen here is consistent with continuous recrystallization to some extent during TMP. Those areas that were not continuously recrystallized or sufficiently recovered during TMP could have had a discontinuous recrystallization process triggered by the rapid heating. This model accounts for the finding of recovered areas comprising subgrain structure only, as well as refined moderate- and high- angle boundary regions, and even regions of large grains in the same specimen. The isolated large grains would have little impact on hardness, but would certainly be detrimental to superplastic properties. Finally, because the microstructure is essentially the same after long-term aging, it is concluded that continuous recrystallization does not occur during aging.

Munro [Ref. 35] conducted TEM examinations of the tensile test specimen grip sections of the three low lithium content alloys. Despite comparable times at temperature, the microstructure he found differed significantly from that of the coupons of this work. The microstructure he found was much more homogeneous, and more suggestive of a continuously recrystallized structure. There was no evidence of large grains, nor was the area fraction of recovered microstructure significant. Thus the heating rate may be an important factor in microstructural development, and must be carefully controlled during TMP and subsequent material evaluation.

B. 8%MG-0.5%LI, 8%MG-1%LI, AND 6%MG-1%LI ALLOYS

The low lithium alloys showed no evidence of a significant age hardening response, nor was δ' found by SADP or by the DSC research of Munro [Ref. 35]. The absence of δ' is consistent with the findings of Fridlyander referred to in Chapter II [Ref. 25]. It has been suggested that age hardening may be possible in alloys with lithium content as low as 1% when accompanied by magnesium to reduce the lithium's solid solubility. Munro's DSC data on these alloys suggest the reverse may be true; the lithium reduces the magnesium solubility, increasing the size of the β peak of the 8%Mg-1%Li alloy over that of the 8%Mg-0.5%Li alloy [Ref. 35]. While showing no significant hardening response, the low lithium alloys also showed no softening or grain growth during prolonged heat treatment, indicating a stable microstructure. This stability, coupled with their fine microstructure, explains the excellent superplastic response found in the work of Munro, in which the 8%Mg-1%Li alloy sustained elongations in excess of 1000% [Ref. 35]. Despite the lack of a significant age hardening response, these alloys are fine grained, highly superplastic, and have no continuous grain boundary phases. They have moderate strength due to grain size effects and solid solution strengthening. For comparison, assuming that aluminum alloys of the same hardness have the same ultimate tensile strength (σ_{uts}), yields a σ_{uts} for the 8%Mg-1%Li alloy of 380 MPa, putting it about midway between 5056-H38 at 414 MPa, and 5456-H116, at 352 MPa [Ref. 42: p.5]. Considering the effect of density by comparing the values of σ_{uts} divided by density however, finds the strength density ratio of the 8%Mg-1%Li alloy only 4% lower than 5056, and 12% better than 5456, which is used in many applications, including pressure vessels, and for marine structures.

The ternary phase diagram for the Al-Mg-Li system, and the apexes of the ternary phase fields appear in Figure 2 and Table 2 respectively. Values in Table 2 for

300°C were obtained by interpolation, those for 150°C, by extrapolation [Ref. 16: p.307]. The data for point C are suspect due to the unknown nature of the changes in lithium solubility in β and in $Al_{12}(Mg,Li)_{17}$ with temperature. It is believed that the Al + $Al_{12}(Mg,Li)_{17}$ phase field may cease to exist at low temperature. At equilibrium conditions at 150°C, phases present are Al, Al_2MgLi, and β. Non-equilibrium phases, formed during TMP, such as $Al_{12}(Mg,Li)_{17}$, may persist indefinitely. No multi-constituent intermetallic phases were found, leading to the conclusion that these alloys behave like quasi-binary Al-Mg alloys, with the lithium staying in solution and acting as a density reducing, minor alloying element only.

The delayed age hardening response of the 6%Mg-1%Li is apparently not due to the precipitation of δ'. In the 6%Mg-2%Li alloy with a somewhat larger degree of hardening (the 10 hour samples), δ' was easily found. The formation of G.P. zones has been found in Al-Li alloys [Ref. 43], but significant hardening due to their formation has not been proposed.

More Al_3Zr was found in the 6%Mg-1%Li alloy, due to its almost double concentration of zirconium. The amount of secondary Al_3Zr precipitated is dependent on the casting. Higher superheat suppresses formation of primary Al_3Zr, leaving more zirconium in solution to precipitate in the secondary form, which may be identified by its non-homogeneous distribution, spheroidal morphology, and small size.

C. 6%MG-2%LI ALLOY

Analysis of the Al-Mg-Li phase diagram (Figure 2) for 150°C indicates that the equilibrium second phase will be Al_2MgLi. This is consistent with experimental evidence. Also present is the metastable δ'. The presence of multi-constituent intermetallic phases makes this a true ternary alloy, and explains some of the differences found between it and the lower lithium alloys, which behaved as quasi-binaries.

The annealed hardness of the 6%Mg-2%Li alloy is almost identical to that of the two 8%Mg alloys. This is consistent with their very similar alloy contents, in atomic percent. The drop in hardness evident at 0.3 hours is not uncommon in age hardening aluminum alloys. It is due to reversion, the process in which clusters which had formed around dislocations during the quench, revert into solution, driven by surface energy, and triggered when the aging temperature provides activation energy for diffusion [Refs. 44,45]. By one hour's aging, a hardening response is apparent. The curve is almost a 'classic' age hardening response, in which a lower temperature's curve

peaks more slowly, but reaches a higher peak, than the higher temperature. The apparent inversion of the two curves between 0.7 and 7 hours is most likely due only to the scatter of data, which is only accurate to about 5%. The 480-hour samples came out of the furnace too late to examine by TEM for the effects of δ' coarsening, volume fraction, PFZ's, and Al_2MgLi precipitation. The 150 C, 168-hour metallography wafer suffered from surface contamination, which precluded direct comparison with the significantly harder 120 C sample.

Hardening over time in the 6%Mg-2%Li alloy is due entirely to the precipitation of a fine, uniform dispersion of δ'. There is no significant change in the grain size, nor in the other second phases, which are much more coarse, and unevenly distributed. The hardnesses of the two 10-hour samples are virtually identical, however, there is a noticeable difference in the δ' distributions (see Figures 4.24 and 4.28). The lower temperature specimen's particle size (about 3 nm) appears to be smaller by about half, but the spacing is closer. The two opposing factors seem to cancel. Fridlyander found peak hardness to correspond to δ' particle size of 25-35 nm [Ref. 25: p. 94]. By 168 hours (see Figure 4.32), the δ' has coarsened to about 20 nm, still less than Fridlyander's peak, and consistent with the curve's upward trend. The volume fraction is hard to determine, but appears on the order of 0.33. A lever rule calculation using the δ' solvus data from Sigli and Sanchez [Ref. 22] in Figure 2.2 yields a weight fraction of about 24% for the 120°C aged condition. In the absence of density data for δ', approximating its density from atomic mass and lattice parameter results in a volume fraction of about 30%, consistent with experimental findings.

The age hardening of Al-Mg-Li alloys has been investigated by others not concerned with its implications to superplasticity. Dinsdale, *et al.* [Ref. 46], investigated the effects of magnesium content on a 2%Li alloy. Aged at 170 C, their 6%Mg-2%Li-0.2%Zr alloy's peak strength was 460 MPa, slightly less than the estimated peak of 483 MPa of this work. They found peak hardness to occur for the 4%Mg-2%Li, and concluded that there was little utility in magnesium additions above that level. Increased magnesium content is critical in the NPS alloys with respect to β precipitation for grain refinement. Noble, *et al.* [Ref. 47], aged a 4%Mg-2%Li alloy to a peak strength σ_{uts} of 510 MPa at 195°C. This is consistent with Dinsdale's finding of higher strength in that alloy than in the higher magnesium one. Parson and Sheppard [Ref. 48] aged a similar alloy 16 hours at 170° C, and attained peak strength in the range 500-520 MPa. They found δ' to precipitate in the matrix, and Al_2MgLi to

precipitate on the grain boundaries. The lack of grain boundary precipitation significant to mechanical properties in this research is due to the lower temperature, and to the increased boundary surface area spreading the precipitates out. Harris, *et al.* [Ref. 49], in a continuation of Dinsdale's work on the 4%Mg-2%Li alloy, found that a 10% stretch before aging increased σ_{uts} 5-7%. They also found significant benefit in cold rolling prior to aging, yielding hardnesses up to 25% higher than those attained without cold work. It is not feasible to stretch a superplastically formed part prior to aging, so that the SPF part to be aged must rely on the dislocations remaining from the TMP and SPF to replace those that would result from cold work. Harris, *et al.*, aged at several temperatures, two of which were 125°C and 150°C, which allow direct comparison with the results of this work. After 24 hours aging, their alloy attained hardnesses about 15% higher than those achieved in this research. In an assessment of fracture toughness, they found the underaged condition to be optimal for their 6%Mg-2%Li alloy. K_Q and K_{IC} values lie within the range of those of the 2xxx alloys.

The rolling difficulties with the 6%Mg-2%Li alloy, found also by Lee [Ref. 50], have several possible explanations. They could be due to inadequate control of impurities, which was investigated with energy dispersive x-ray spectroscopy analysis of the fractured sample. Excessive amounts of calcium were found, but this result is questionable. The problems could also be a result of the TMP. Three different temperatures were tried, but all resulted in fractures. A more extensive study of TMP variables, to include temperature, reduction per pass, total rolling strain, and reheat time between rolling passes, needs to be conducted. The problem could also be inherent in the alloy itself, so that, whatever the TMP used, rolling below the β solvus to the large strains used for the lower lithium alloys may be impossible.

The peak hardness of the 6%Mg-2%Li is slightly higher than that of 2024-T3. Making the same assumption used for the 8%Mg-1%Li alloy comparison, that aluminum alloys of the same hardness have the same σ_{uts}, yields a σ_{uts} for the 6%Mg-2%Li alloy of 485 MPa, about 15% less than 7075-T6 [Ref. 42: p.7]. Considering the effect of density by comparing the values of σ_{uts} divided by density, finds the strength density ratio of the 6%Mg-2%Li alloy 13% higher than 2024, and only 2% less than 7075. Both alloys are widely used in aerospace applications calling for high strength.

According to Chellman [Ref. 5] of Lockheed-California, an aerospace industry goal is to achieve a density of 2.5 g cm^3 in a structural alloy. At a density of 2.45 g cm^3, with strength equal to 2024, and with the potential for superplastic forming, the 6%Mg-2%Li alloy may be an attractive candidate.

VI. CONCLUSIONS

The following conclusions are drawn from this study:

1. The 8%Mg-0.5%Li and 8%Mg-1%Li alloys are non-age hardening, low density alloys of moderate strength. When thermomechanically processed as in this work, they have a stable, fine microstructure capable of sustaining superplastic elongations in excess of 1000% at relatively low temperature and high strain rates.
2. The alloys containing 1% or less lithium behave as quasi-binary aluminum-magnesium alloys. β precipitating during rolling serves to retard grain growth, producing highly refined microstructure. No δ' nor multi-constituent intermetallic compounds precipitated in these alloys.
3. The microstructure of the annealed coupons contained regions of recovered substructure, regions of fine, continuously recrystallized grain structure, and regions of coarse, discontinuously recrystallized grains. This microstructure is not the same as that of tensile test grip sections due to the triggering of discontinuous recrystallization by the significantly higher heating rate experienced by the coupons.
4. The 6%Mg-2%Li alloy behaved as a ternary alloy, precipitated no β, and had a somewhat different microstructure than the lower lithium alloys. Dispersed and grain boundary intermetallics are suspected of contributing to the cracking experienced on rolling. The relatively fine and stable microstructure, and the highly superplastic response of the lower lithium content alloys suggest that superplastic behavior is likely after a more suitable TMP.
5. Heating rate during and after processing is a significant factor in the development of microstructure capable of sustaining superplastic deformation.
6. The 6%Mg-2%Li alloy experienced a significant age hardening response due to the precipitation of δ'. At 150°C, peak hardness of 72 HRB was attained in ten hours. At 120°C, hardness was 78 HRB and still increasing after 480 hours.

VII. RECOMMENDATIONS

The following topics are recommended for further study:

1. Conduct an investigation to determine the reason for the hardening response found in the 6%Mg-1%Li alloy after long term aging at 120°C.
2. Design a TMP suitable for the 6%Mg-2%Li alloy.
3. Conduct age hardening studies of specimens which have been superplastically deformed to determine the effect of deformation on the age hardening response.
4. Experiment with alloy composition to find the line of demarcation between quasi-binary and true ternary alloys, and between those that age harden, and those that do not.
5. Conduct an investigation into the role of heating rate in the development of microstructure by the NPS process.

APPENDIX
HARDNESS DATA

TABLE 3

8%MG-0.5%LI HARDNESS DATA

Annealed Hardness 54.6 HRB

Time (hours)	Hardness (HRB)	
	Aged at 100°C	Aged at 120°C
0.3	54.1	53.1
1	54.1	54.6
3	53.8	54.0
10	54.1	54.5
24	54.5	54.3
72	53.6	53.4
168	52.5	54.1

TABLE 4

8%MG-1%LI HARDNESS DATA

Annealed Hardness 52.6 HRB

Time (hours)	Hardness (HRB)	
	Aged at 100°C	Aged at 120°C
0.3	56.4	56.0
1	57.2	56.1
3	56.9	55.6
10	53.3	57.3
24	55.5	54.4
72	55.2	55.7
168	53.1	56.4

TABLE 5

6%MG-1%LI HARDNESS DATA

Annealed Hardness 46.6 HRB

Time (hours)	Hardness (HRB)	
	Aged at 120°C	Aged at 150°C
0.3	46.7	46.3
1	47.1	45.7
3	47.0	47.3
10	47.0	47.5
24	46.6	48.1
72	47.2	49.1
168	49.5	50.3
480	55.7	47.3

TABLE 6

RECRYSTALLIZED 6%MG-1%LI, AGED AT 150°C, HARDNESS DATA

Time (hours)	Hardness (HRB)	
	Recrystallized at 350°C	Recrystallized at 450°C
No aging	36.3	35.7
0.3	38.2	37.6
3	40.6	36.3
24	41.5	36.7
168	46.4	40.6

TABLE 7

6%MG-2%LI HARDNESS DATA

Annealed Hardness 54.3 HRB

Time (hours)	Hardness (HRB)	
	Aged at 120°C	Aged at 150°C
0.3	44.8	50.9
1	59.1	57.1
3	67.8	64.4
10	70.2	71.3
24	73.3	70.7
55	73.7	70.5
168	75.7	69.9
480	77.6	65.0

LIST OF REFERENCES

1. Quist, W.E., Narayanan, G.H., and Wingert, A.L., "Aluminum-Lithium Alloys for Aircraft Structure - An Overview," *Aluminum-Lithium Alloys II*, Sanders, T.H., and Starke, E.A., eds, pp.313-334, The Metallurgical Society of AIME, 1984.

2. Starke, E.A., Sanders, T.H., and Palmer, I.G., "New Approaches to Alloy Development in the Al-Li System," *Journal of Metals*, pp. 24-32., August, 1981.

3. Balmuth, E.S., and Schmidt, R. "A Perspective on the Development of Aluminum-Lithium Alloys," *Aluminum Lithium Alloys*, American Society for Metals, pp. 69-88, 1982.

4. Anderton, D.A., "Tomorrow's Fighter: Updated or Outdated," *Aviation Week and Space Technology*, pp. 61-102, August 10, 1987.

5. Chellman, D.J., "Al-Li IM and PM Forging Alloys for Aircraft Applications," paper presented at the Fourth International Al-Li Conference, Paris, June 10, 1987.

6. Roeder, J., keynote address presented at the Fourth International Al-Li Conference, Paris, June 10, 1987.

7. Oster, S.B., *Effect of Thermomechanical Processing on the Elevated Temperature Behavior of Lithium-Containing High-Mg, Al-Mg Alloys*, Master's Thesis, Naval Postgraduate School , Monterey, California, June 1986.

8. Sanchez, B.W., *Processing and Superplasticity in Lithium-Containing Al-Mg Alloys*, Master's Thesis, Naval Postgraduate School, Monterey, California, March 1987.

9. Meyers, M.A., and Chawla, K.K, *Mechanical Metallurgy*, Prentice-Hall, 1984.

10. Barrett, C.R., Nix, W.D., and Tetelman, A.S., *The Principles of Engineering Materials*, Prentice-Hall, 1973.

11. Humphreys, F.J., "The Nucleation of Recrystallization at Second Phase Particles in Deformed Aluminum," *Acta Met.*, Vol. 25, pp. 1323-1344, 1977.

12. Cotteril, P., and Mould, P.R., *Recrystallization and Grain Growth in Metals*, pp. 266-325, John Wiley and Sons, 1976.

13. Nes, E., "Recrystallization in Alloys with Bimodal Particle Size Distributions," *Recrystallization and Grain Growth in Multi-Phase and Particle Containing Materials*, Hansen, N., Jones, A.R., and Leffers, T., eds., Riso National Laboratory, pp. 85-95, 1980.

14. Grimes, R., "The Manufacture of Superplastic Alloys," *Superplasticity*, pp. 8.1-16, Advisory Group for Aerospace Research and Development, NATO, 1987.

15. *Metals Handbook, Desk Edition*, American Society for Metals, 1985.

16. Mondolfo, L.F., *Aluminum Alloys: Structure and Properties*, Butterworths, 1976.

17. Murray, J.L., "Al-Mg Phase Diagram" *Binary Alloy Phase Diagrams*, Massalski, T.B., ed., p. 130, American Society for Metals, 1986.

18. Samson, S., "The Crystal Structure of the Phase β Mg_2Al_3," *Acta Crystallographica*, Vol. 19, pp. 401-413, 1963.

19. Lee, E.W., McNelley, T.R., Stengel, A.F., "The Influence of Thermomechanical Processing Variables on Superplasticity in a High-Mg Al-Mg Alloy," *Met. Trans. A*, Vol. 17A, pp. 1043-1050, 1986.

20. Hales, S.J., Oster, S.B., Sanchez, B.W., and McNelley, T.R., "Grain Refinement and Superplasticity in a Lithium Containing Aluminum-Magnesium Alloy by Thermomechanical Processing," *Acta Met.*, to be published.

21. Gu, B.P., Liedl, G.L., Sanders, T.H., and Weldmann, K., "The Influence of Zirconium on the Coarsening of δ' (Al_3Li) in an Al-2.8wt.%Li-0.14wt%Zr Alloy," *Materials Science and Engineering*, Vol. 76, pp. 147-157, 1985.

22. Sigli, C., and Sanchez, J.M., "Calculation of Phase Equilibrium in Al-Li Alloys," *Acta Met.*, Vol.34, No.6, pp. 1021-1028, 1986.

23. McAlister, A.J., "Al-Li Phase Diagram," *Binary Alloy Phase Diagrams*, Massalski, T.B., ed., p. 128, American Society for Metals, 1986.

24. Sanders, T.H., and Starke, E.A., "Overview of the Physical Metallurgy in the Al-Li-X Systems" *Aluminum-Lithium Alloys II*, Sanders, T.H., and Starke, E.A., eds., pp. 1-15, The Metallurgical Society of AIME, 1984.

25. Fridlyander, A.N., Sandler, V.S., and Nikol'skaya, T.I., "Investigation of the Ageing of Aluminum-Magnesium-Lithium Alloys" *Phys. Met. Metallog.*, Vol. 32, pp. 93-100, 1971.

26. Gu, B.P., Mahalingam,K., Liedl, G.L., and Sanders, T.H., "The δ' Particle Size Distribution in a Variety of Al-Li-Zr Systems," *Aluminum-Lithium Alloys III*, pp. 360-368, The Institute of Metals, 1986.

27. Gayle, F.W., and Vander Sande, J.B., "Composite Precipitates in an Al-Li-Zr Alloy," *Scripta Met.*, 18, pp. 473-478, 1984.

28. Hatch, J.E., ed., *Aluminum: Properties and Physical Metallurgy*, p. 51, American Society for Metals, 1984.

29. Thompson, G.E., and Noble, B., "Precipitation Characteristics of Aluminum-Lithium Alloys Containing Magnesium," *Journal of the Institute of Metals*, Vol. 101, pp. 111-115, 1973.

30. Luo, H., Chao, C.C., and Duwez, P., "Metastable Solid Solutions in Aluminum-Magnesium Alloys," *Transactions of The Metallurgical Society of AIME*, Vol. 230, pp. 1488-1490, 1964.

31. Noble, B., Harris, S.J., and Dinsdale, K., "The Elastic Modulus of Aluminum-Lithium Alloys," *The Journal of Materials Science*, Vol. 17, pp. 461-468, 1982.

32. Bauman, S.F., and Williams, D.B., "The Effect of Ternary Additions on the δ' α Misfit and the δ' Solvus Line in Al-Li Alloys," *Aluminum-Lithium Alloys II*, Sanders, T.H., and Starke, E.A., eds., pp. 17-29, The Metallurgical Society of AIME, 1984.

33. Anamet Laboratories, Inc., Berkeley, CA. laboratory report of January 23, 1986.

34. ASTM Standard E18, "Standard Methods for Rockwell Hardness and Rockwell Superficial Hardness Testing of Metallic Materials," *ASTM Annual Standards*, American Society for Testing and Materials, 1986.

35. Munro, I.G., *Optimizing Superplasticity in Lithium Containing Aluminum-Magnesium Alloys*, Master's Thesis, Naval Postgraduate School, Monterey, California, December 1987.

36. *Metals Handbook*, 9th ed., Vol. 9, pp. 351-360, American Society for Metals, 1985.

37. Edington, J.W., *Practical Electron Microscopy in Materials Science*, Vol. 2, Philips Eindhoven, 1975.

38. Noble, B., and Thompson, G.E., "Precipitation Characteristics of Aluminum-Lithium Alloys," *Metal Science Journal*, Vol. 5, pp. 114-120, 1971.

39. Williams, D.B., and Edington, J.W., "The Precipitation of δ' in Dilute Aluminum-Lithium Alloys," *Metal Science* Vol. 9, pp. 529-532, 1975.

40. Villars, P., and Calvert, L.J., *Pearson's Handbook of Crystallographic Data for Intermetallic Phases* Vol. 2, American Society for Metals, 1985.

41. Loretto, M.H., *Electron Beam Analysis of Materials*, Chapman and Hall, 1984.

42. *Source Book on Selection and Fabrication of Aluminum Alloys*, American Society for Metals, 1978.

43. Papazian, J.M., Sigli, C., and Sanchez, J.M., "New Evidence for GP Zones in Binary Al-Li Alloys," *Scripta Met.*, Vol. 20, pp. 201-206, 1986.

44. Christian, J.W., "Phase Transformations," *Physical Metallurgy*, Cahn, R.W., ed., p.541, American Elsevier, 1965.

45. Smallman, R.E., *Modern Physical Metallurgy*, p.409, Butterworths, 1962.

46. Dinsdale, K., Harris, S.J., and Noble, B., "Relationship Between Microstructure and Mechanical Properties of Aluminum-Lithium-Magnesium Alloys," *Aluminum-Lithium Alloys*, Sanders, T.H., and Starke, E.A., eds., pp. 101-118, The Metallurgical Society of AIME, 1981.

47. Noble, B., Harris, S.J., and Harlow, K., "Mechanical Properties of Al-Li-Mg Alloys at Elevated Temperatures," *Aluminum-Lithium Alloys II*, Sanders, T.H., and Starke, E.A., eds., pp. 65-77, The Metallurgical Society of AIME, 1984.

48. Parson, N.C., and Sheppard, T., "The Effect of Process Parameter on the Microstructure and Properties of an Al-Li-Mg Alloy," *Aluminum-Lithium Alloys II*, Sanders, T.H., and Starke, E.A., eds., pp. 219-237, The Metallurgical Society of AIME, 1984.

49. Harris, S.J., Noble, B., and Dinsdale, K., "Effect of Composition and Heat Treatment on Strength and Fracture Characteristics of Al-Li-Mg Alloys," *Aluminum-Lithium Alloys II*, Sanders, T.H., and Starke, E.A., eds., pp. 219-237, The Metallurgical Society of AIME, 1984.

50. Lee, E.W., Naval Air Development Center, Warminster, PA, unpublished research, 1987.

INITIAL DISTRIBUTION LIST

		No. Copies
1.	Defense Technical Information Center Cameron Station Alexandria, VA 22304-6145	2
2.	Library, Code 0142 Naval Postgraduate School Monterey, CA 93943-5002	2
3.	Department Chairman, Code 67Pl Department of Aeronautics Naval Postgraduate School Monterey, CA 93943-5000	1
4.	Department Chairman, Code 69Hy Department of Mechanical Engineering Naval Postgraduate School Monterey, CA 93943-5000	1
5.	Professor T. R. McNelley, Code 69Mc Department of Mechanical Engineering Naval Postgraduate School Monterey, CA 93943-5000	5
6.	Dr. S. J. Hales, Code 69He Department of Mechanical Engineering Naval Postgraduate School Monterey, CA 93943-5000	3
7.	Naval Air Systems Command, Code AIR 931A Naval Air Systems Command Headquarters Washington, DC 20361	1
8.	LCDR W. F. Ferris, USN Patrol Squadron 31 NAS Moffett Field, CA 94035	5
9.	Dr. E. W. Lee, Code 6063 Naval Air Development Center Warminster, PA 18974	1
10.	LCDR S. B. Oster, USN 110 Terry Ct. NE Bremerton, WA 98310	1

END
DATE
FILM
4-88
DTIC